LBL-10737

Lawrence Berkeley Laboratory
UNIVERSITY OF CALIFORNIA

Materials & Molecular
Research Division

MASTER

TOUGHENING OF ZIRCONIA COMPOSITES

Nicholas Hamilton Bl[illegible]ingame
(M.S. thesis)

June 1980

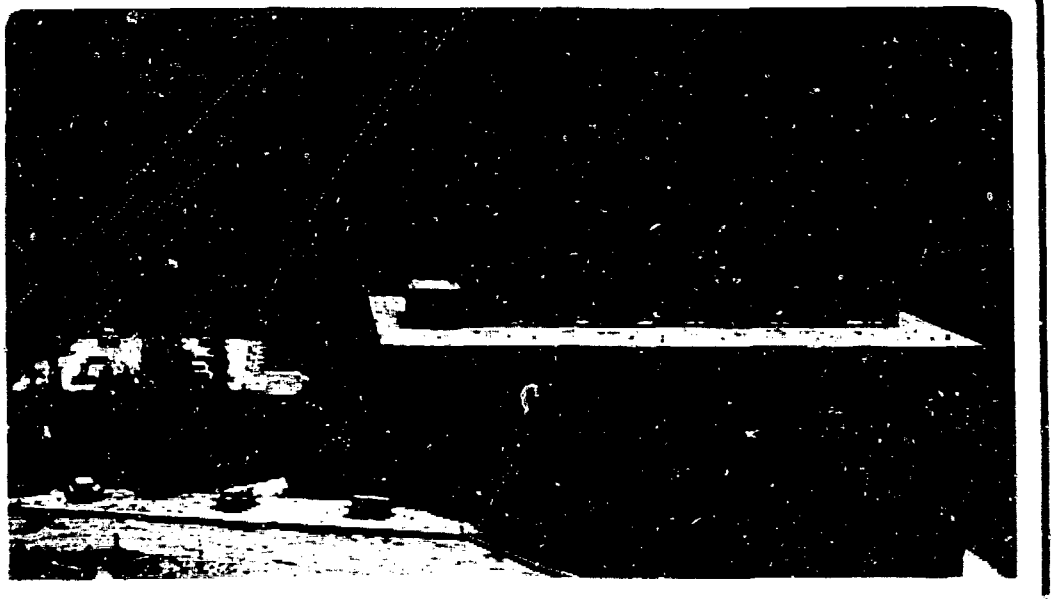

Prepared for the U.S. Department of Energy under Contract W-7405-ENG-48

Table of Contents

Table of Contents

TOUGHENING OF ZIRCONIA COMPOSITES

Nicholas Hamilton Burlingame

Materials and Molecular Research Division
Lawrence Berkeley Laboratory
and
Department of Materials Science and Mineral Engineering
University of California, Berkeley, California 94720

ABSTRACT

The addition of a ZrO_2 dispersion can significantly enhance the toughness of a ceramic matrix material. The toughness improvement is due to a stress reduction at the tip of a propagating crack which is the result of a preferential martinsitic transformation of ZrO_2 particles in the stress field of the crack. From thermodynamic considerations and experimental observations the toughening effect is shown to be strongly dependent on the ZrO_2 particle size. The effect of variations in temperature, composition and matrix materials are demonstrated, and analyzed in respect to the resultant deviations in the particle size toughening effect.

I. INTRODUCTION

Improved toughness of ceramic materials has been attained by utilizing a tetragonal to monoclinic phase transformation present in the ZrO_2 system.[1-4] The high temperature tetragonal phase can be retained in a stable form on cooling if a sufficient elastic constraint is applied by a surrounding matrix. However in the stress field of a propagating crack, the constraint will be relaxed and the possibility of transformation exists.[5] This stress induced transformation is accompanied by a size and shape change which will increase the strain energy in the vicinity of the crack, thus inhibiting further crack growth. Use of this phenomenon has been shown effective for P.S.Z.[3] (with tetragonal precipitates in a cubic matrix) and in a polycrystalline form.[4] Also partially stabilized and unstabilized ZrO_2 have been shown to toughen Al_2O_3 matrix material.[1-2]

In all cases there was found to be a critical size at which the ZrO_2 particles would spontaneously transform on cooling. The critical size may be altered by changes in temperature, additions of stablizing agents and variations in matrix materials employed. This indicates the stability of the ZrO_2 particles is dependent on both chemical and physical variables. The ability to change the critical size has previously been used as a method to retain greater amounts of tetragonal phase (assuming that the amount of retained tetragonal phase is of primary importance). Only limited attention has been devoted to size effects with respect to transformation in the stress field of a propagating crack. However since the stability of the tetragonal ZrO_2 particles varies with their size it follows that their transformation at

a propagating crack will also be a function of particle size. Therefore transformation toughening should include particle size effects with the concomitant implications for composition, temperature and matrix related trends.

Described is an analysis[6] which defines the size stability effect for tetragonal ZrO_2 particles, constrained by a surrounding matrix. The model also provides for the altering of the particles stability in the stress field of a propagating crack; thereby allowing prediction of the degree of transformation and hence, the toughness improvement.

II. THEORY

The fracture toughness of a material can be considered to depend on its ability to absorb energy at a crack tip. A mechanism which proves effective in enhancing the toughness is the preferential transformation of tetragonal ZrO_2 particles to monoclinic, at a propagating crack tip. This transformation is martensitic in nature and is accompanied by a shape and volume change. On transformation there is an increase in the strain energy of the particle-matrix system and a tensile stress reduction at the crack tip. This stress reduction inhibits further crack growth.

The transformation has the following characteristics. The tetragonal structure, if unconstrained becomes unstable at a certain temperature (transformation temperature) and will transform on cooling to the moroclinic structure. However if the tetragonal particles are included in a matrix they will remain stable below the unconstrained transformation temperature whenever the increase in strain is greater than the chemical driving force for transformation. Subsequently in the tensile stress field of a propagating crack, the constraint on the ZrO_2 can be sufficiently reduced that transformation will occur.

The toughening that can be achieved in the presence of a crack tip transformation zone can be analyzed by examining the thermodynamic changes that accompany the transformation process.

A. Transformation Thermodynamics

The transformation of ZrO_2 particles (from a tetragonal to monoclinic crystal structure) constrained by a matrix, is controlled both

by the dispersion of particles and by the matrix properties. The energetics of transformation consist of chemical, surface and strain energy terms. Factors affecting these energy terms are temperature, composition particle size and the relationships between thermal and elastic properties of the particles and the matrix. The role of each of these terms will be discussed in the subsequent sections. Special attention will be devoted to the volume or area dependence of each term because this will be the basis for defining size stability effects.

1. Chemical Free Energy

The tetragonal phase is stable above an unconstrained transformation temperature, and this temperature is reduced by addition of stabilizing agents (Y_2O_3, MgO, CaO). However at lower temperatures there is a chemical driving force for conversion to the monoclinic structure, which is opposed by increases in the strain and surface energies which result from the transformation. The lower the temperature the larger the counteracting energy terms must be in order to maintain the tetragonal phase.

These factors are a function of the free energy difference between unit volumes of the product and parent phases (ΔG). For a spherical particle the chemical free energy change (ΔG_c) is given by;[6]

$$\Delta G_c = -\frac{4}{3}\pi a^3 \Delta G_o \qquad (1)$$

where a is the particle radius. This relation indicates that the chemical driving force is volume controlled.

2. Surface Energies

On transformation there are two sources of surface energy change. One is related to a change at the particle-matrix interface, and the other associated with the formation of variant boundaries within the particles (Fig. 1). These energies are related (for a spherical particle) by the equation;[6]

$$\Delta S = 4\pi a^2\left(\Gamma_i + \frac{a}{3d}\,\Gamma_t\right) \tag{2}$$

with d being the variant spacing, Γ_i the particle-matrix interfacial energy and Γ_t the variant interface (habit plane) energy. Γ_i and Γ_t are small because the monoclinic and tetragonal phases have similar surface energies, and because the variant boundaries are of low energy. This consideration indicates that the surface energy term will be significant only for particles with a large number of variants. It is also noted that the variant boundary energy term depends on the particle volume if the variant spacing is particle size independent as experimental evidence would suggest.[6]

3. Macroscopic Strain Energy

A volume increase and overall shape change accompanies transformation to the monoclinic phase. For a spherical particle the macroscopic strain energy (ΔU_m) is given by;[6]

$$\Delta U_m = (4/3)\pi a^3\left[\Delta V(.14\Delta V - p^A) + \left(.21 E e^{*T}_{ij}\, e^{*T}_{ij} - p^{*A}_{ij}\, e^{*T}_{ij}\right)\right] \tag{3}$$

where V is the volume strain, e^{*T}_{ij} the macroscopic shear strain, p^A the dilational applied stress and p^{*A}_{ij} the deviatoric applied stress.

ZrO_2 particles have been observed to transform at crack tips by means of a series of variants (Fig. 1) with alternating shear strains.[7] The macroscopic shear deformation for this mode is thus negligible, and only the volume strain need be considered. If particle-matrix elastic modulus mismatch is also considered then the final result (for $\nu = 0.2$) becomes;[6]

$$\Delta U_m = \frac{4}{3}\pi a^3 \left[\frac{E_p \beta V}{3.6(1+\beta)} - p^A \Delta V\right] \tag{4}$$

there β is the ratio of matrix to particle elastic modulus. A further adjustment considers the influence of the thermal expansion mismatch. This modification leads to an effective volume strain (ΔV_{eff});

$$\Delta V_{eff} = \Delta V - 3\Delta\alpha\Delta T \tag{5}$$

where; $\Delta\alpha = \alpha_{particle} - \alpha_{matrix}$ and ΔT is the cooling range from the fabrication temperature.

4. Twinning Strain Energy

The twin (or variant) related strain energy derives from the stresses at the particle-matrix interface caused by twinning (these stresses are limited to the interface regions due to the alternating shears between variants). Since the stresses are confined to a zone close to the interface, the twinning strain energy (ΔU_T) is approximately related to the surface area of the ZrO_2 particle (The larger the number of twins (variants) the more accurate this assumption). For a spherical particle;

$$\Delta U_T = (4/3)\pi a^3 E \gamma_T^2 \left[0.32/(1.2 + a/d)\right] \tag{6}$$

where γ_T is the unconstrained shear strain associated with each twin. This expression is adjusted for elastic mismatch between the matrix material and the ZrO_2 particles by assuming an average shear modulus ($<\mu>$);[6]

$$\Delta U_T = \frac{.32 <\mu> (\gamma_T)^2 \Delta V}{1.2 + a/d} \tag{7}$$

where V is the particle volume.

B. Size Effects

An upper bound for the critical transformation size is obtained when the summation of the previously described terms is zero;

$$\Delta U_T + \Delta U_m + \Delta S + \Delta G_c = 0 \tag{8}$$

The principle reason for the existence of this critical size is associated with the twin strain energy term. The magnitude of this term is surface area dependent;† this dependence allows the summation of the strain energy terms (ΔU_T, ΔU_m) to predominate at small sizes, preventing transformation. However, at larger sizes the effect of the free energy terms, which is volume dependent, will favor transformation.

The critical size (a*) obtained by neglecting the macroscopic particle shear and the surface energy terms, as noted above, is given by;[6]

$$a^* = n_c \left(\frac{d}{2}\right) = \frac{0.28\ E_p (1+\beta) \gamma_T^2}{\Delta G_o - 0.28 \beta E_p \Delta V^2/(1+\beta)} \tag{9}$$

---

†Also the twin spacing has been observed to be size independent.[6]

where n_c is the number of variants in the particle at its critical size. Since the stability of a particle is related to its size its response to an applied stress (and hence its toughening effect) will also be size dependent.

C. Transformation Toughening

The toughening effect of ZrO_2 particles will depend on the degree of transformation at the crack tip. This will depend on the number of particles, their stability and the magnitude of the stress field at the crack tip. Therefore the toughening will depend on the ZrO_2 volume fraction and size as well as the matrix toughness.

From the thermodynamic conditions discussed in the previous section, combined with the stress field of a crack tip, a toughness model[12] was derived. The toughening effect for a single particle size is given[12]

$$\frac{\Gamma_T}{\Gamma_o} = \frac{1}{1 - \varepsilon} \tag{10}$$

where

$$\varepsilon = 2L \left(\frac{\Delta V}{V_T}\right)^2 V_f \frac{(2.4 + n_c)(2.4 + n)}{(n_c - n)} \tag{11}$$

where Γ_T is the composite toughness, Γ_o the matrix toughness and L is a stress relaxation term which allows for stress reduction due to prior transformation nearer the crack.

To make the situation more realistic a particle size distribution ($\Phi(a)\,da$) is included. An extreme value distribution is assumed for $\Phi(a)\,da$; chosen because the larger particles will contribute most

significantly to the toughness. Also, this particular distribution has been found to correlate well with the size distribution of microstructural entities[8] (e.g. grain size). This frequency function is given by;

$$\phi(a)\,da = \frac{a_o^k}{a^{k+1}} \exp.\left[-\left(\frac{a_o}{a}\right)^k\right] da \qquad (12)$$

where a_o is a scale parameter given by;

$$a_o = \bar{a} / \Gamma(1 - 1/k) \qquad (13)$$

and $\bar{a}$ is the average radius (volume distribution) and k is a shape parameter. The toughness equation is now modified by;

$$\epsilon = 2\omega \frac{(\Delta V)^2}{\gamma_T} V_f (2.4 + n_c) \left[\frac{1}{\langle a^3 \rangle} \int_o^{a^*} \frac{a^4 \Phi(a)\,da}{a^* - a}\right] \qquad (14)$$

where a* is the critical radius for spontaneous transformation. The integral can be solved numerically for various values of a_o/a^* and k. The number of variants at the critical size (n_c) can be calculated, and the remaining terms are obtained from previous studies.[6]

An effective experimental comparison with the model may be achieved from the comparison of the trends in the amount of spontaneously transformed monoclinic phase and the toughness. The comparison is possible because both are functions of the particle size distribution. By assuming the same distribution function noted above the volume ratio of monoclinic phase is given by;

$$\frac{V_{MONO}}{V_{TOTAL}} = \frac{\int_{a^*}^{\infty} a^3 \phi(a) da}{\langle a^3 \rangle} \qquad (15)$$

The combination of toughness versus distribution and toughness versus monoclinic content provides two methods of comparison with experimental data.

III. EXPERIMENTAL

The initial section will describe sample preparation and testing procedures common to the majority of specimens evaluated. Subsequent sections will describe additions and deviations from the general procedure for each compositional series.

A. General Procedure

a) Powder Preparation. Two methods were used to prepare power with a well dispersed ZrO_2 phase. The first consisted of the direct mixing of oxides, incorporating long milling times, and high-purity media of the same composition as the matrix phase. The milling process was limited to Al_2O_3-ZrO_2 composites, for which Al_2O_3 media* is acceptable. The oxides were milled for 24 hrs. on a SWECO** vibratory mill in polyethelene bottles containing isopropyl alcohol. The second method was a gel technique in which various salts were used as precursors for their oxides. This method represented an attempt to retain the inherently excellent dispersion of an aqueous solution. Zirconal Acetate† and aluminum sulfate†† were the basis of the gel formation. Other salts present which do not gel would be trapped in the gel structure, thereby preventing migration (this effect pertains because the entire solution is included within the gel).

---

*Coors Hi-Purity Al_2O_3 media

**SWECO Inc.

†Orion Chemical Co.

††Baker Chemical Co.

Solutions in which zirconal acetate controlled the pH (e.g. no Al^{+3} ions) could be thermally gelled. For uniform gelling this was accomplished by heating in a microwave oven. Gels which contained both zirconal acetate and aluminum sulfate were formed by the addition of NH_4OH, while rapidly stirring. This was necessary because the aluminum sulfate increased the acidity of the solution and eliminated the possibility of thermal gelling.

The gels were either freeze dried or thermally dried. Thermal drying resulted in rather strongly aggregated powders, whereas the freeze drying yielded powders with an extremely low bulk densities. After drying, the resultant powders were decomposed to their oxides by calcining between 800 and 850°C in a furnace with flowing oxygen. Powders with aluminum sulfate were calcinated at 850°C for 2 hrs.; otherwise calcination was conducted at 800°C for 1 hr.

b) Hot Pressing. One inch disk specimens were formed by vacuum hot pressing. Graphite dies, containing the powders, were heated with molybdenum resistance heating elements. Shrinkage of the disks was recorded by means of a displacement transducer. These measurements allowed a reasonably accurate monitoring of the density and hence, permitted the use of minimal temperatures (to attain full density).

The hot pressing schedule consisted of heating at 1000°C/hr. to 700°C, holding for 1 hr., followed by heating at the previous rate until the pressure was applied. At this point the heating rate was reduced to 750°C/hr. Pressures of 5000 psi were slowly applied when the first noticeable shrinkage occurred. The maximum temperature essentially corresponded with the temperature attained at the termination of shrinkage.

The milled Al_2O_3-ZrO_2 composites were fired to 1410°C, while the chemically prepared Al_2O_3-ZrO_2 materials were fired to 1450°C (there was no hold at maxi temperature in these cases).

c) Surface Preparation. The condition of the surface is critical to the evaluation of the properties of materials containing tetragonal ZrO_2. Specifically the extent of stress induced transformation due to grinding will determine whether surface dominated rather than bulk properties are being observed. Samples were ground and polished on a high-speed surface finishing device.* Both surfaces were rough ground, with a 90 μm diamond wheel to yield flat and mutually parallel surfaces. Specimens were then polished in successive steps with a 15 μm diamond wheel, followed by 6, 1, and 1/4 μm diamond pastes (pastes were carried by rosewood pegs). The polish was considered sufficient when x-ray diffraction indicated that the amount of the monoclinic phase was similar to that in the as fired state. After polishing, samples were annealed at 1250°C for 1/2 hr. (above the transformation temperature).

d) Indentation. Fracture toughness measurements were obtained directly by indentation[9] and also by a bi-axial bend test on disks containing indention pre-flows. Polished specimens were indented with a Vickers diamond indentor mounted on a table model Instron. A crosshead speed of .05 cm/min was used. Peak loads of 50 kg were used for Al_2O_3 composites and 25 kg for the mullite materials. Indentation toughness was also measured for samples at several stages of the polishing procedure. For this purpose loads ranging from 2-50 kg were used to

---

*Strugers; Pedipin

permit the cracks to sample various depths beneath the surface. After indentation the cracks were stained with an ink marker which allowed excellent visibility under polarized light.

Optical micrographs of the indentations (Fig. 2a) were used to determine the indentation size (2a) and the crack length (2c) (Fig. 2b). K_{IC} was calculated from c/a using the relation developed by Evans and Charles.[9] The results for three indentations per sample were averaged, and only symmetrical indentations were considered.

The specimens used for the pre-crack, toughness determinations were polished and annealed after indentation to eliminate both residual stresses and the transformation zone at the pre-cracks. Finally these specimens were fractured at a series of temperatures. The fracture experiments were conducted using a bi-axial flexure method. The fixture (Fig. 3) was constructed from Al_2O_3, hot pressed to shape in preformed graphite dies. Calculation of the fracture stress (σ_f) was achieved using the relation;[10]

$$\sigma_f = \frac{-3}{4\pi} \frac{P}{d^2} (X-Y) \tag{16}$$

where;

$$X = (1 + \nu) \ln(B/C)^2 + \left[(1 - \nu)/2\right](B/C)^2$$

$$Y = (1 + \nu)\left[1 + \ln(A/C)^2\right] + (1 - \nu)(A/C)^2$$

F is the load applied at fracture, d is the thickness of the specimen, ν is Poisson ratio, B is the radius of the loaded area, C is the radius of the specimen, and A is the radius of the support circle. The load was applied through alumina pushrods which were enclosed in a furnace.

The load was applied at a crosshead speed of .05 cm/min in an Instron testing machine. From the fracture stress, K_{IC} measurements could be obtained using the equation;[11]

$$K_{IC} = Y_f M(2) \sqrt{c/\pi} \tag{17}$$

where c is crack depth, and M is a free surface correction factor. The crack size was measured before and after fracture; the measurements were self-consistent. The shape of the cracks were easily established, by employing a crack pre-straining procedure (Fig. 4). M was then estimated from the flow shape.

e) X-ray diffraction. The amount of monoclinic phase (X_m) was calculated from the relation;[12]

$$X_m = \frac{I_m(111) + I_m(11\bar{1})}{I_m(111) + I_m(11\bar{1}) + I_T(111)} \tag{18}$$

where $I_m(111)$ and $I_m(11\bar{1})$ are the integral intensities for the corresponding monoclinic peaks and $I_T(111)$ for the tetragonal peak. When estimation of the bulk monoclinic content was desired, polished and annealed samples were analyzed (The monoclinic content in polished and annealed specimens was lower than in the as fired state). Similar samples were used for matrix phase identification.

f) S.E.M. Polished, etched and fracture surfaces were observed by scanning electron microscopy. This provided information about the particle size distribution, shape and dispersion. Extreme value particle size distributions were measured by recording the areas of the largest

ZrO_2 grain within sampling areas of 26 μm^2. For this purpose several micrographs of polished surfaces were examined.

B. Compositional Series

a) Al_2O_3-ZrO_2. Powders were prepared by the milling of oxides. The ZrO_2 was formed by calcining zirconal acetate. X-ray diffraction showed that the resultant powder was ~100% tetragonal, indicating the formation of aggregates with a small crystallite size.[13] This ZrO_2 was milled together with a sub-micron Al_2O_3*, after which the dried powders contained only monoclinic ZrO_2. This indicates that the intensive milling procedure was effective in de-aggregating the ZrO_2 (by the complete degree of the stress induced transformation).

b) Al_2O_3-P.S.Z. CaO, MgO and Y_2O_3 were added in various percentages to produce partially stabilized zirconias. The CaO and MgO doped zirconias were combined at a volume fraction of .15 with Al_2O_3, while Y_2O_3-ZrO_2 combinations were prepared at volume fractions of .2a and .42 with Al_2O_3.

CaO and MgO additions were in the form of nitrates**. These were added to aqueous solutions of zirconal acetate, thermally gelled and dried. The powder was then pre-reacted by calcining a 800°C for 1 hr. The resultant powder was milled together with Al_2O_3.

Al_2O_3-ZrO_2 (yttrium stabilized) composites with a volume fraction of .29 ZrO_2 were formed from solutions of aluminum sulfate, yttrium

---

*Union Carbide; Linde A

**Baker Chemical Co.

acetate* and zirconal acetate. These solutions were gelled, freeze dried, and calcined. The powders were hot pressed at two temperatures (1450°C (no hold) and 1550°C (1.5 hr. hold)) to achieve different particle sizes.

Composites with a volume fraction of 0.42 were prepared by milling ZrO_2** (Stabilized with 4 wt.% Y_2O_3) along with Al_2O_3. This powder provided specimens for pre-crack toughness measurements.

c) $\underline{Al_2O_3\text{-}SrZrO_3}$. $SrZrO_3$ was prepared from strontium nitrate+ and zirconal acetate solutions, which were thermally gelled and dried. Powders were calcined to form $SrZrO_3$ and milled together with Al_2O_3. Powders were hot pressed to 1475 (with no soak).

d) $\underline{\text{Mullite-}ZrO_2}$. Two types of powders were prepared by different methods; one used Al_2O_3++ powder and the other aluminum sulfate. Both were calculated to form mullite containing 73 wt.% Al_2O_3 (slight excess of Al_2O_3).

Al_2O_3 powder was mixed with colloidal SiO_2† and zirconal acetate in water. The slurry was thermally gelled, dried, and calcined. The powder was hot pressed at 1550 °C for 1.5 hrs. (Series 1).

---

*(rion Chemical Co.

**Zircar Corp.

+Baker Chemical Co.

++Atomeric Chemical Company

†Ludox AS-40

Aluminum sulfate was combined with colloidal silica, and zirconal acetate in water. The mixture was gelled with NH_3OH and freeze dried. This powder was hot pressed at 1450°C for 1 hr (Series 2) and then annealed at 1550°C for 1.5 hrs. (Series 3).

IV. EXPERIMENTAL RESULTS

A. Hardness

The hardness values were relatively invariant for the mullite-ZrO_2 materials, as was that for the Al_2O_3-ZrO_2 materials with a volume fraction of ZrO_2 less than 0.15. However, the hardness diminished at greater volume fractions (Fig. 6). Materials with the lower hardness values were also very friable (Fig. 5).

B. Toughness vs. Volume Fraction

a) Mullite-ZrO_2. Three series of mullite materials with varying amounts of ZrO_2 were examined. The first (Series 1) yielded an excellent dispersion of ZrO_2 particles (Fig. 7-9). The resultant distribution of ZrO_2 was quite narrow ($k = 10$, $b_o = .35$ for a volume fraction of .16) with a limited amount of aggregration. The toughness and tetragonal phase content are plotted as a function of the ZrO_2 volume fraction (Fig. 10). This plot indicates an increase in toughness and a decrease in the proportion of the tetragonal phase as the volume fraction increases.

The second (Series 2) consisted of a much finer dispersion of ZrO_2 particles. Toughness and diffraction measurements indicate negligible toughening and complete retention of the tetragonal phase (Fig. 11). However, annealing above the fabrication temperature to induce grain growth (Series 3) yielded materials with a higher toughness (with and without ZrO_2) while maintaining full retention of the tetragonal phase (Fig. 11). Comparison of the first two series (Series 1 and 2)

illustrates that the course grained material exhibits greater toughness improvements (Fig. 12).

b) $\underline{Al_2O_3\text{-}ZrO_2}$. The trends in toughness* and tetragonal content as a function of volume fraction (Fig. 13) indicate a peak toughness occurring at a volume fraction of 0.15 and a monotonic decrease in the retained tetragonal phase. Measurements of the size distributions of ZrO_2 particles obtained on polished surfaces (Fig. 14 and 15) indicate both a change in average size and in shape factor (Fig. 16). However, examination of etched surfaces indicates the larger grains contain several particles (Fig. 17) (The distribution parameters pertinent for comparison with the model require isolated particles decreasing the reliability of direct comparisons).

C. Toughness vs. Composition

Additions of CaO and MgO, to $Al_2O_3\text{-}ZrO_2$ (at a ZrO_2 volume fraction of .15) caused a decrease in toughness while increasing the proportion of the retained tetragonal phase (Fig. 18-19).

Samples containing 0.29 volume fraction ZrO_2 (Fig. 20) with various amounts of Y_2O_3 were fabricated at two temperatures. Toughness for the material fabricated at low temperatures exhibited a maximum for low amounts of Y_2O_3, whereas the maximum was shifted to higher Y_2O_3 content for the samples fired at the higher temperature (Fig. 22-24). In both cases the amount of the tetragonal phase increased with Y_2O_3 content.

---

*Indentations were not stained for the milled $Al_2O_3\text{-}ZrO_2$ series causing an overestimation of K_{IC} values.

D. Toughness vs. Temperature

The dependence of the toughness (for a material with .42 volume fraction ZrO_2 stabilized with 4 wt.% Y_2O_3 (Fig. 21) decreases monotonically with an increase in temperature (Fig. 25).

E. Toughness vs. Surface Compression

Samples formed from $SrZrO_3$ and Al_2O_3 after hot pressing consisted of $6Al_2O_3 \cdot SrO$, Al_2O_3 and ZrO_2 (the ZrO_2 was predominately of the tetragonal phase). K_{IC} measurements (for a 50 Kg indentation load) are given verses volume fraction for a rough polished (15 μm grit) surface and for the same surface after annealing (Fig. 26). This indicates a large change in the surface toughness with abrasion.

During various stages of polishing a sample containing 0.21 volume fraction ZrO_2 was analyzed for the amount of tetragonal phase present and the effective toughness (employing several indentation loads) (Fig. 27). The toughness is also presented as a function of depth (Fig. 28).

V. DISCUSSION

A. General Consideration

Examining the toughness equation; (refer to Eqs. 10-14)

$$\Gamma/\Gamma_o = \frac{1}{1-\epsilon}$$

where;

$$\epsilon = \langle\omega\rangle\left(\frac{\Delta V}{V_T}\right)^2 V_f(2.4 + n_c)\ I \qquad (19)$$

allows the prediction of toughness trends. Analysis of the integral, I, is presented as a function of size, normalized by the critical size (Fig. 29). This is directly related to the enhancement in toughness due to tetragonal ZrO_2 dispersions. Since this term is dimensionless it may be used to illustrate general trends. The k-values used in calculation of I, represent the width of the distribution (a large k indicates a narrow distribution), while the average size ($\bar{a}$) is represented by the scaling factor, a_o.

The results of the calculations indicate a narrow size range in which the toughness may be significantly improved. The peak toughness is highest and the effective range smallest for narrow distributions. There is also a shift in peak values with variations of k (because $\bar{a} \approx a_o$ for large k and $\bar{a} > a_o$ for smaller k).

The amount of monoclinic ZrO_2 which forms on cooling is calculated as a function of the normalized size distribution. This is then compared with the calculated values of I to determine the toughness trends in relation to monoclinic phase content (Fig. 30). These results indicate

that an appreciable amount of monoclinic phase must be present before there is any significant increase in toughness. The peak toughness values occur at monoclinic contents of 75% and greater. These predictions are not consistent with observations (Fig. 11-13). Reasonable toughness values have been obtained for materials with no monoclinic (Fig. 13) phase present and peak toughness values obtained at monoclinic contents from 25-50% (Fig. 13, 22-24). This indicates that the present model does not consider certain important toughening factors.

Deviations from the model at smaller sizes could be due to particles at or near a free surface having a lower constraint imposed by the matrix; hence also a lower critical size. Therefore the stability of a particle may depend on its distance from the free surface created by the crack (as well as the constraint reduction due to the stress field of the crack). This effect would diminish as the distance between the crack and the particle increases and would be insignificant as distances greater than one particle diameter. Considering that observed[19] transformation zone sizes (.6 μm for P.S.Z.). are very small, this factor needs consideration. (This however would not alter the general trends as the particle stability would still be a strong function of particle size). The effect of a reduced constraint at a free surface is supported in that diffraction experiments on annealed polished surfaces yield much lower monoclinic contents than annealed rough surfaces. Also a source of underestimation may be due to particles in the bulk material being thermodynamically unstable with respect to transformation in the step mode, but requiring the presence of a high shear force (as is present with a propagating crack) to nucleate transformation.

Another phenomenon neglected in the model is microcracking. This process is also a size dependent effect, manifested in a critical size for spontaneous microcracking.[14] Also it has been postulated that the microcracks will form in the stress field of a crack and will have a toughening trend similar to that previously described (in that it will exhibit the same size dependence indicated by the factor I). However the microcracking critical size is significantly larger than the critical size for transformation[2,3,15] (for isolated particles). Also it is anticipated that the critical size will decrease with increases in volume fraction of ZrO_2. These suggest that there should be little or no effect due to microcracking at small sizes (low monoclinic contents) and low volume fractions of ZrO_2, but at larger sizes and volume fractions microcracking may occur. However since the size range of interest (for transformation toughening) is small, microcracking in these cases would be due to particle interactions. Hence microcracking linking is quite possible. If this degrades the matrix toughness (Γ_o) then the ZrO_2 additions would have an adverse toughening effect. Microcracking could therefore determine the peak toughening effect which would vary with ZrO_2 particle size and volume fraction.

The effect of altering the matrix toughness is another aspect demonstrated by the toughness equation in that the resultant toughness is directly proportional to the matrix toughness. Suggesting that the improvement in toughness will be influenced by the choice of the matrix material and its microstructure details (such as grain dimensions).

The use of this model allows prediction of toughness trends with regard to temperature, composition and matrix variations. By recognizing the size effect, and assuming an upper limit, (where microcracking will begin to degrade the toughness) factors which alter the standard free energy (ΔG_o) can be explained by their effect on the critical size. Referring back to the equation defining the critical size (a*);

$$n_c = \frac{2a^*}{d} = \frac{0.14E_p(1+\beta)\gamma_T^2}{\Delta G_o - 0.28\beta E_p \Delta V^2/1+\beta}$$

demonstrates that a* will increase with a reduction of ΔG_o (increase in temperature, or addition of stablizing agent) or an increase in matrix modulus. Also comparison with the toughness equation indicates that an increase in the critical size (which is also an increase in n_c) will allow a higher toughness, with proper adjustment of the size distribution. The trends which could be expected for variations of ΔG_o and matrix modulus are demonstrated (Fig. 31-32). These trends suggest that methods of preparation and the choice of material can be used to greatly alter the toughness. Also for any material the optimum temperature range will be limited and cooling below this range will adversely effect the toughness.

These predictions may be altered by microcracking effects. These effects would be related to particle size and volume fraction, with larger sizes and higher volume fractions leading to a larger degree of microcracking. This effect would define a particle limit on the critical size which may effectively be employed. (Also the variation in critical size might prove effective in optimizing microcrack toughening effects).

In the subsequent section results of calculations for mullite and Al_2O_3 matrix materials, with ZrO_2 dispersions, are presented. These are compared with measured toughness and size information. For these calculations it is assumed that $\gamma_T \sim .14$[6], $\Delta V \sim .058$, and $\Delta G_o \sim 230$ MPa. The effective volume change (ΔV_{eff}) was calculated by taking into account the differential thermal expansion between particle and matrix. For the proportionality constant (ω), which takes into account stress reduction due to prior transformation, a value of .4 was used. This value is determined from comparison of a calculation zone size of 1.5 μm[6] and a measured zone size of .6 μm.[3] This size was considered constant for all cases even though the measured zone corresponds to a cubic ZrO_2 matrix with a high volume fraction of tetragonal ZrO_2. Since this factor depends on the degree of transformation at the crack tip it will most likely be a function of volume fraction.

B. Specific Toughening Effects

a) Size and Volume Fraction Effects

Additions of unstabilized ZrO_2 as a toughening agent, to various matrix materials, is usually limited to low volume fraction.[16,19] This limitation is attributed to the complication that increases in the volume fraction of ZrO_2 may cause increases in the ZrO_2 particle size. Therefore, in examining data in which the volume fraction is varied the possibility of size changes must also be considered.

The Al_2O_3-ZrO_2 system (Fig. 13) covers a wide enough range in ZrO_2 volume fraction to show the complete cycle of a large toughness improvement followed by a subsequent decline. Neglecting any effects

of particle interactions it can be assumed that the increase in the percent of monoclinic phase present relates to the growth of the ZrO_2 particles. Thus appearance of the spontaneously transformed particles infers a decrease in their stability. This decrease corresponds to a rapid increase in toughness as the percent of the monoclinic phase increases. However as the volume fraction, and hence the monoclinic fraction, is further increased the toughness diminishes rapidly. The decline in toughness occurs at much lower monoclinic contents than predicted by the model. This decrease is therefore assumed due to a large degree of microcracking degrading the matrix. Supporting this assumption are the trends in hardness (Fig. 6), notably the constancy of hardness of monoclinic contents up to the maximum toughness value followed by a sharp decline. The decrease in hardness indicates microcracking as the rapid decline is much more severe than would be expected solely from the addition of a softer phase. Other indications of microcracking are the friable nature as evidenced by the inability to polish the surface to a smooth finish (Fig. 5).

Trends for a mullite ZrO_2 material (Series 1) were similar, in that the toughness rose sharply with increases in the volume fraction and monoclinic content (Fig. 10). However the volume fraction range wasn't extended to the region where a noticeable drop in hardness and toughness could be expected (although the rate of toughness improvement did decline).

Numerical analysis of the predicted toughness values (as a function of a_o/a^* and monoclinic content) compared with experimental data for the Al_2O_3-ZrO_2 (Figs. 33-36) and mullite-ZrO_2 (Fig. 37-38) systems yielded

similar trends. Comparison of measured toughness values with predicted values would suggest that the average size remains constant (Figs. 33-34, 37) with volume fraction (experimental K_{IC} values intersect their corresponding toughness curves at the same a_o/a^* value). However such constancy is not observed, as evidenced by size data (Figs. 7-8, 16) and monoclinic content increases. Comparison with predicted toughness values based on the monoclinic content (Figs. 35-36, 38) indicate that the effect of the smaller size range is greatly underestimated. It is also suggested that the stress relaxation term (ω) may be an inverse function of volume fraction. Error in this term could account for errors in the higher monoclinic content materials (at larger volume fraction). However, the major weakness appears to be the underestimate of the toughness values at smaller particle sizes.

Since there is the possibility of some ambiguity when explaining size effects while varying volume fraction ZrO_2, two mullite-ZrO_2 materials with similar volume fractions and different size distributions were compared (Fig. 12). This figure demonstrates that toughness may vary greatly by alteration of only the particle size. The point is very strongly demonstrated as the finer grained material (Fig. 11) shows almost no toughness improvement with large volume fractions of ZrO_2. Also the ZrO_2 is totally retained in the tetragonal form thereby proving that the amount of toughening agent is of importance only if the size distribution is also optimized. Extending this range to include another size distribution (Series 3), which also has total retention of the ZrO_2 in the tetragonal phase, again demonstrates that significant toughening effects occur in the size range below that predicted by the model.

b) Matrix Effect

Al_2O_3 as a matrix material has a much larger elastic modulus than mullite, explaining the larger critical size for the Al_2O_3 materials. Also, the Al_2O_3 material would have a higher matrix toughness. These factors cannot be separated, but it is evident (Fig. 13, 10) that the Al_2O_3 materials have a larger toughening response (for materials with similar volume fraction of ZrO and monoclinic content).

The matrix effect could be isolated by altering the matrix toughness without changing the composition. This was accomplished by observing a mullite-ZrO_2 system before (Series 2) and after annealing (Series 3). By annealing an unexpected effect occurred, this being an increase in the matrix toughness. This alteration may be due to change in particle aspect ratio or size causing a toughening effect related to the "pullout" of elongated grains. Another possibility is a chemical composition shift. However due to the very fine microstructural scale direct evidence supporting either of these conjectures was unobtainable. (This result is quite significant as the toughness was increased by 60% with no additions and warrants further investigation). Even though this effect isn't readily explainable it may still be used to demonstrate the effect of altering matrix toughness. The predicted effect is supported in that the material with the higher matrix toughness has much greater toughness increases with ZrO_2 addition (There is also the possibility of toughening due to ZrO_2 particle growth, this is however presumed small as the material is still 100% tetragonal).

C. Compositional and Temperature Effects

The addition of stabilizer to materials for which the optimum toughening was not exceeded, caused a decrease in toughness and an increase in the percent of retained tetragonal (Fig. 18-19). This demonstrates that although a stabilizing agent allows an increase in the amount of toughening agent (tetragonal ZrO_2) it will still result in a decrease in toughness, unless accompanied by a corresponding size increase. However if the size is altered to optimize the toughness (Fig. 24) higher values are achieved for increased stabilizer content (The method of varying ZrO_2 particle size by increasing sintering temperatures may also alter the distribution shape or degree of aggregation). Also it is shown that the toughness may be improved by an increased retention of tetragonal phase if the optimum toughening situation is exceeded (Fig. 22-24).

An increase in temperature has an effect similar to the addition of a stablizing agent. For a material with a high tetragonal content it is demonstrated (Fig. 25) that the toughness will decrease as the temperature increases. However it is important to note that an extremely high value of toughness (K_{IC} = 8.8 MPa$\sqrt{m}$) was obtained at liquid nitrogen temperature. It is assumed that this value could be translated to room temperature by altering the amount of stabilizer or the size distribution.

Another noteworthy item in this experiment is the testing method. This method would seem effective as similar results are obtained for both the indentation method and when testing toughness by an existing flaw method it is assumed necessary to anneal the samples. Otherwise the toughness may be dependent on the transformation zone induced during

indentation (this is of practical importance in that it suggests that the effective toughness of a material may be a function of the minimum temperature encountered by the material).

Observations of fracture surfaces from these experiments also yield an interesting result. It was found that the crack pre-strain method not only aided in crack length and shape measurements but also yielded information on the size of the plastic zone at the indentation site (See Appendix I).

D. Toughness vs. Surface Compression

Previous discussion concerned toughening due to transformation at the tip of a propagating crack. An indirect method of toughening is also possible, this being due to the formation of a compressive region at the surface. This layer will form on abrasion of the surface by means of a stress induced transformation. The effective toughness (K_{eff}) would be given by;[16]

$$K_{eff} = \frac{2}{\sqrt{\pi}} \sigma_o \sqrt{c} + K_{IC}$$

where σ_o is the stress at the surface.

It is demonstrated that very large improvements are possible due to this effect for relatively large depths (Fig. 25, 28). Also it is shown that the effect is very strongly related to the depth and can be calibrated with respect to x-ray diffraction data (Fig. 27). Another important aspect is the choice of material. The choice was made as the material ($6Al_2O_3 \cdot SrO$, Al_2O_3, ZrO_2) demonstrated the highest change in toughness (and also in monoclinic phase content) on grinding. The reason

isn't clear as the bulk toughness is much lower than for other materials tested. This indicates that the transformation due to surface abrasion may be quite different from that expected at a crack tip.

E. Microstructural Development

Since the properties of these material are extremely sensitive to particle size and composition the ability to control the microstructure and doping uniformity is to great importance.

The gel preparation proved very effective in allowing addition of dopants, as demonstrated by the ability to produce $SrZrO_3$ at low temperatures (800°C). Also the uniformity of the dispersions (Figs. 7-9) indicates the high homogeneity of material formed from this method. This technique was especially useful in the fabrication of mullite-ZrO_2 materials (Series 1-3). It allow the preparation of materials with high contents of unstablized ZrO_2 (in the tetragonal form).

Another point of practical interest is the ability to limit grain growth by additions of ZrO_2 dispersions. The grain growth control increases with the volume fraction ZrO_2 (Figs. 39-43) while causing a simultaneous increase in ZrO_2 particle size (Fig. 7-8). The growth control is assumed due to a grain boundary drag effect or an alteration in grain boundary diffusion (since the ZrO_2 lies on the boundaries).

IV. SUMMARY

Toughening due to the martensitic transformation of ZrO_2 in the stress field of a propagating crack is predicted to be strongly dependent on the ZrO_2 particle size distribution. This prediction is confirmed experimentally, however the degree and the limits are not clearly defined. The effects of variation in composition, temperature, and matrix modulus are demonstrated to alter the stability of the ZrO_2 particles. This permits analysis in terms of a size toughening effect, allowing prediction of optimum conditions.

The effect of surface transformation is also shown useful as a means of toughening ceramic materials. This is limited to surface properties, but is effective at depths comparable to typical surface flaws.

ACKNOWLEDGMENTS

The author wishes to thank Professor Anthony G. Evans for his guidance and encouragement through the course of this work. Further thanks are extended to Professor Alan Searcy and Lutgard DeJonhe. Finally I would like to express appreciation to my fellow students.

This work was supported by the Division of Materials Sciences, Office of Basic Energy Sciences, U. S. Department of Energy under contract No. W-7405-ENG-48.

APPENDIX I

When a brittle material is indented (with a sufficient load) a zone of plastic deformation is formed near the indentation site.[16] This results in the formation of large residual stresses and a series of cracks emanating from the elastic-plastic interface.[17] This effect can be correlated to the response of ceramic material subject to fatigue[18] and abrasion[19] related phenomena.

To characterize the effect of indentations the size and shape of the resultant plastic is necessary. It is demonstrated (Fig. A1-A4) that by impregnating an indentation with an ink and subsequent fracturing of the material (along the radial cracks) that both the plastic zone and the cracks extending from the interface are readily observed.

REFERENCES

1. F. F. Lange, Rockwell Science Center Report SC5117.7TR (1979).
2. N. Claussen, J. Am. Ceram. Soc. 85 (1978).
3. D. L. Porter and A. H. Heuer, J. Am. Ceram. Soc. 62, 298 (1978).
4. F. F. Lange, Tech. Reports 2 and 3, #N00014-17-C-0441 (1978).
5. A. G. Evans and A. H. Heuer, LBL W-7405-ENG-48 (1979).
6. A. G. Evans, N. Burlingame, M. Drory, and W. M. Kriven, ACTA Metallurgica, in press.
7. D. L. Porter and A. H. Heuer, J. Am. Ceram. Soc. 66, 183 (1977).
8. A. G. Evans, B. R. Tittmann, L. Ahlbeqo, B.T. Khuri-Yakub, and G. S. Kino, J. Appl. Phys. 49 (5) (1978).
9. A. G. Evans, "Fracture Mechanics Applied to Brittle Materials," ASTM STP 678, 112-135 (1979).
10. Wachtman, Capps, Mandel, J. of Materials 7, 188 (1972).
11. Task Group E24.07.01.
12. Garvie and Nicholson, J. Am. Ceram. Soc. 55 (6), 303 (1972).
13. Mitsuhashi, Ichehara, Tatsuke, J. Am. Ceram. Soc. 57 (2), 97 (1974).
14. A. G. Evans and K. T. Faber, J. Am. Ceram. Soc., to be published.
15. H. Claussen, J. Am. Ceram. Soc. 59 (1-2), 47 (1976).
16. A. G. Evans, "Fracture Toughness: The Role of Indentation Techniques," Fracture Mechanics Applied to Brittle Materials, ASTM STP 678, 112-135 (1979).
17. B. Lawn, A. G. Evans, D. B. Marshall, "Elastic/Plastic Indentation Damage in Ceramics: The Media/Radial Crack System,"

18. A. G. Evans, "Fatigue in Ceramics," submitted to the International Journal of Fracture.

19. A. G. Evans, "Abrasive Wear in Ceramics: An Assessment," R. W. Rice, editor, National Bureau of Standards Special Publication 562.

FIGURE CAPTIONS

Fig. 1. Transmission electron micrograph of an Al_2O_3/ZrO_2 material containing .42 volume fraction ZrO_2.*

Fig. 2. Same as Fig. 1 at a higher magnification.*

Fig. 3. Schematic of bi-axial bend fixture.

Fig. 4. Optical micrograph of the fracture surface of a pre-flawed bend sample.

Fig. 5. Scanning electron micrograph of "polished" surface of an Al_2O_3/ZrO_2 material with .29 volume fraction ZrO_2 (note friable nature of this material).

Fig. 6. HARDNESS and percent retained tetragonal ZrO_2 as a function of ZrO_2 content.

Fig. 7. Scanning electron micrograph of polished, and etched surface of a mullite material (Series 1) .16 volume fraction ZrO_2.

Fig. 8. Scanning electron micrograph of polished and etched surface of a mullite material (Series 1) with .08 volume fraction ZrO_2.

Fig. 9. A) Same as Fig. 7 at a higher magnification.

B) SEM photograph of fracture surface of a mullite material (series 1) with .16 volume fraction ZrO_2.

Fig. 10. K_{IC} and percent retained tetragonal ZrO_2 vs. volume fraction ZrO_2 for mullite-ZrO_2 series (#1).

Fig. 11. K_{IC} and percent retained tetragonal for mullite/ZrO_2 Series 2 and 3.

Fig. 12. K_{IC} vs. volume fraction ZrO_2 for mullite/ZrO_2, Series 1 and 3

---

*T.E.M. micrographs courtesty of Dr. W. M. Kriven

Fig. 13. K_{IC} and percent retained tetragonal ZrO_2 vs. volume fraction ZrO_2, for Al_2O_3 - ZrO_2 system.

Fig. 14. Scanning electron micrograph of polished surface of a Al_2O_3 material with .15 volume fraction ZrO_2.

Fig. 15. Scanning electron micrograph of Al_2O_3/ZrO_2 material with .08 volume fraction ZrO_2.

Fig. 16. Extreme value size distribution data.

Fig. 17. Scanning electron micrograph of etched surface of Al_2O_3 with .15 volume fraction ZrO_2.

Fig. 18. K_{IC} and percent retained tetragonal ZrO_2 vs. weight percent CaO for a Al_2O_3 material with .15 volume fraction ZrO_2.

Fig. 19. K_{IC} and percent tetragonal ZrO_2 vs. weight percent MgO for a Al_2O_3 material with .15 volume fraction ZrO_2.

Fig. 20. Scanning electron micrograph of Al_2O_3 material with .29 volume fraction ZrO_2 (partially stabilized with 4 weight percent Y_2O_3).

Fig. 21. SEM photograph of Al_2O_3 material with .42 volume fraction ZrO_2 (partially stabilized with 4 weight percent Y_2O_3).

Fig. 22. K_{IC} and percent retained tetragonal vs. weight percent Y_2O_3, for a constant ZrO_2 volume fraction of .29 (Hot pressed at 1450°C).

Fig. 23. K_{IC} and percent tetragonal vs. weight percent Y_2O_3 for a Al_2O_3/ZrO_2 material with .29 volume fraction ZrO_2 (Hot pressed at 1550°C).

Fig. 24. Comparison of Figs. 22 and 23.

Fig. 25. K_{IC} vs. temperature for a Al_2O_3 material with .42 volume fraction ZrO_2.

Fig. 26. K_{IC} vs. volume fraction ZrO_2 for $Al_2O_3/SrZrO_3$ material (with two surface treatments).

Fig. 27. K_{IC} vs. fn (of the monoclinic over tetragonal ratio) for a $Al_2O_3/SrZrO_3$ material with .21 volume fraction ZrO_2.

Fig. 28. K_{IC} vs. Indentation depth (for same material as described for Fig. 27).

Fig. 29. I vs. a_o/a^* (I is directly related to toughness, a_o/a^* is a normalized size function).

Fig. 30. I vs. percent monoclinic ZrO_2.

Fig. 31. K/K_o ($K = K_{IC}$ of material K_o = matrix toughness) vs. a_o/a^* (a_o = size scaling factor, a^* = critical transformation size) for variations in temperature, matrix modulus, and composition.

Fig. 32. K/K_o vs. a_o/a^* for variations in temperature, matrix modulus and composition.

Fig. 33. K/K_o vs. a_o/a^* compared with measured values for an Al_2O_3 - ZrO_2 system ($k = 6$).

Fig. 34. Same as Fig. 22 for a $k = 9$.

Fig. 35. K/K_c vs. percent monoclinic ZrO_2 compared with measured values for an Al_2O_3 - ZrO_2 system ($k = 6$).

Fig. 36. Same as Fig. 35 for a $k = 9$.

Fig. 37. K/K_o vs. a_o/a^* compared with measured values for an mullite-ZrO_2 system (Series 1).

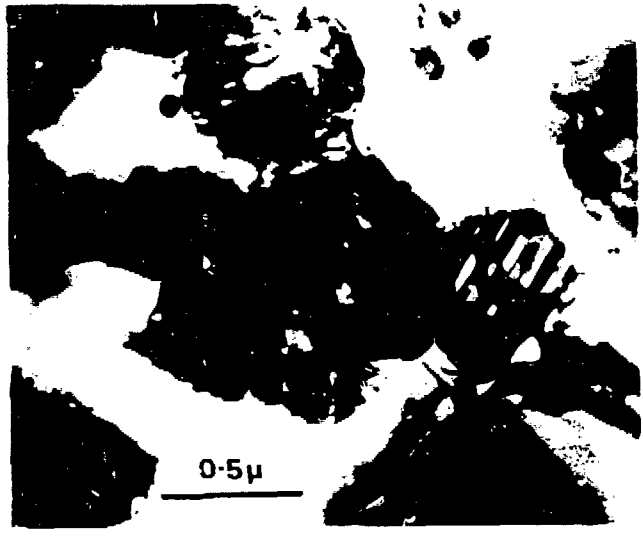

XBB 803-3495

Fig. 1

XBB 803-3494

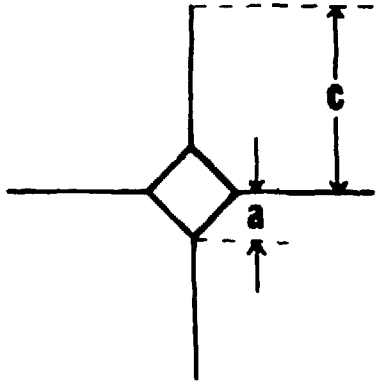

Fig. 2

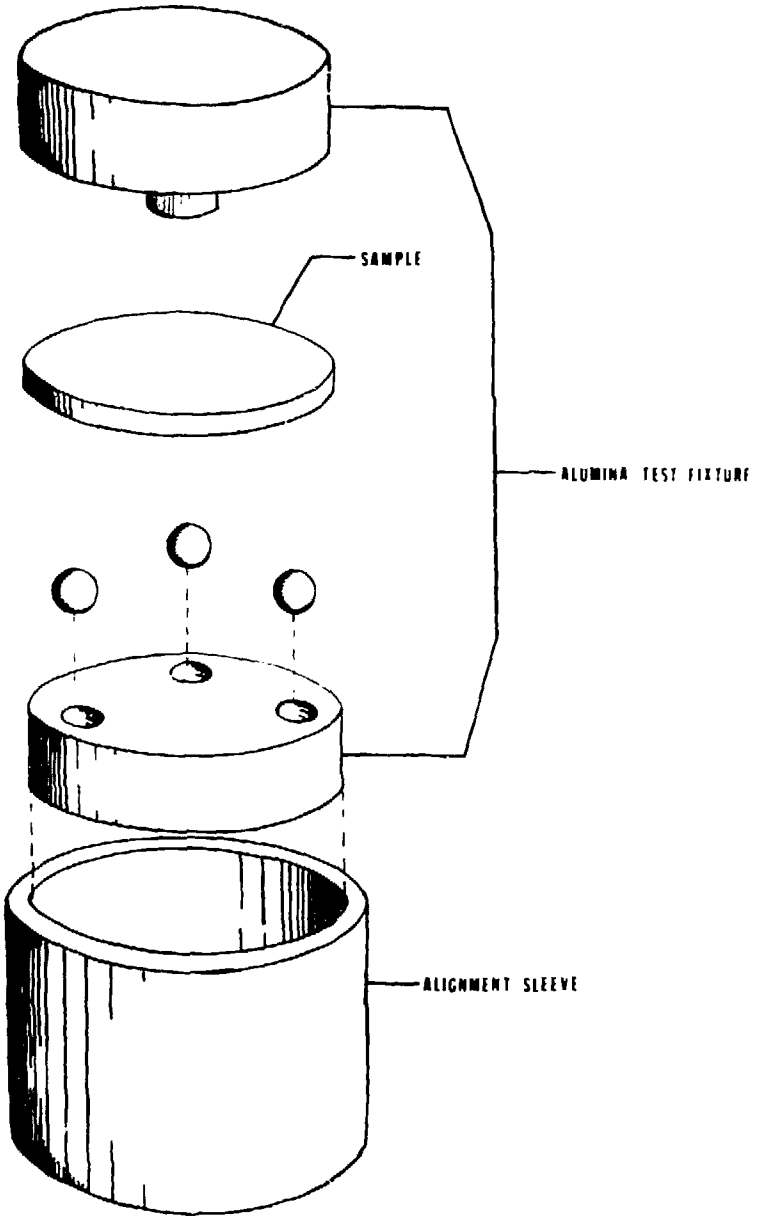

XBL 803-8936

Fig. 3

Fig. 4

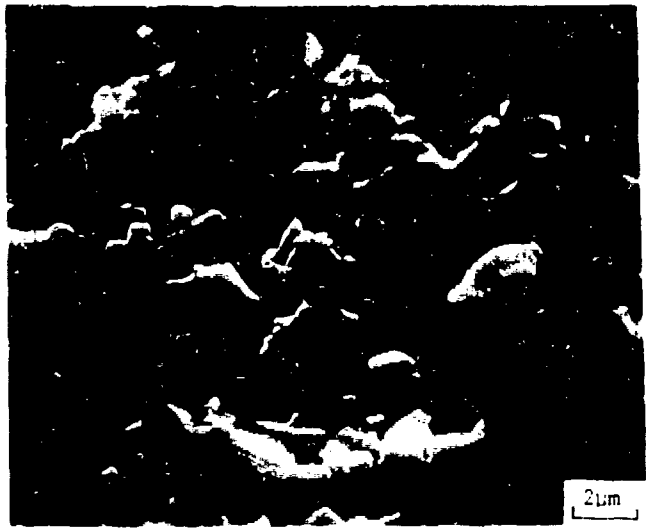

XBB 803-3496

Fig. 5

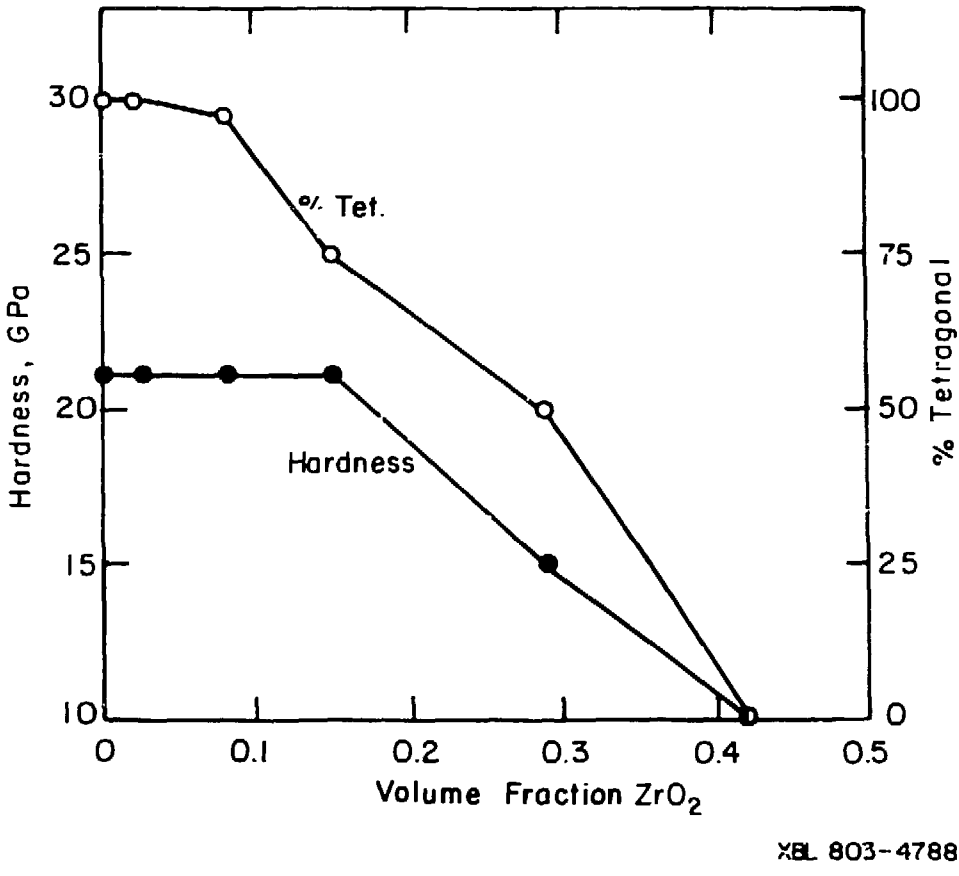
30
25
20
15
10
Hardness, GPa
100
75
50
25
0
% Tetragonal
% Tet.
Hardness
0
0.1
0.2
0.3
0.4
0.5
Volume Fraction ZrO_2
XBL 803-4788

Fig. 6

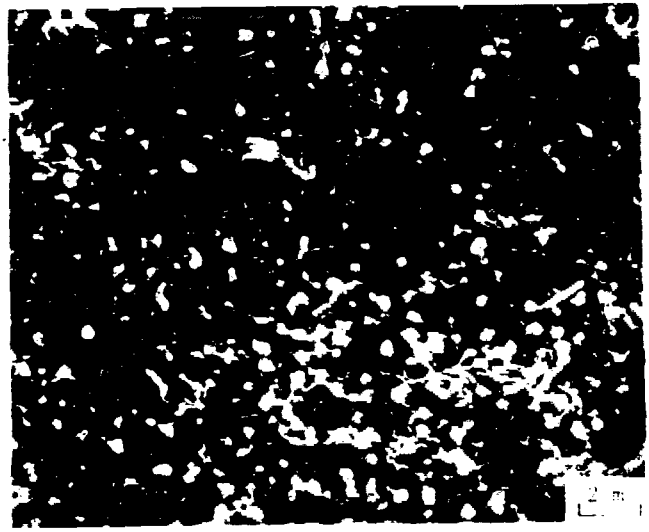

Fig. 7

XBB 803-3497

Fig. 8

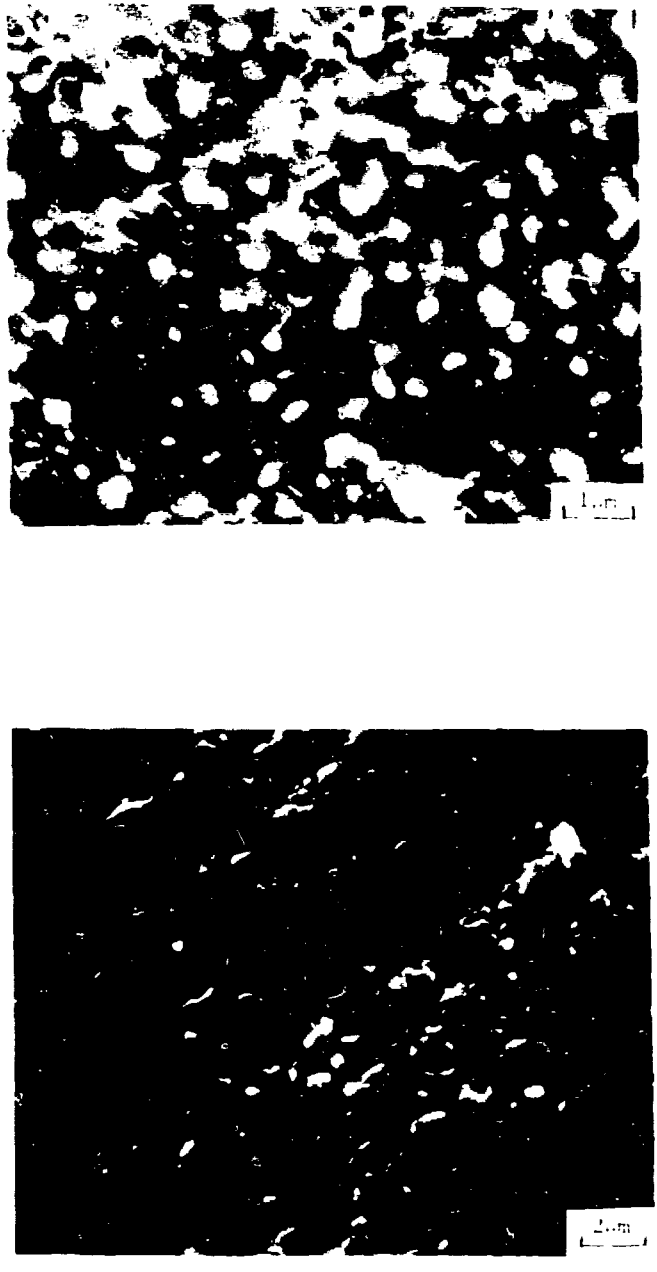

XBB 803-3498

Fig. 9

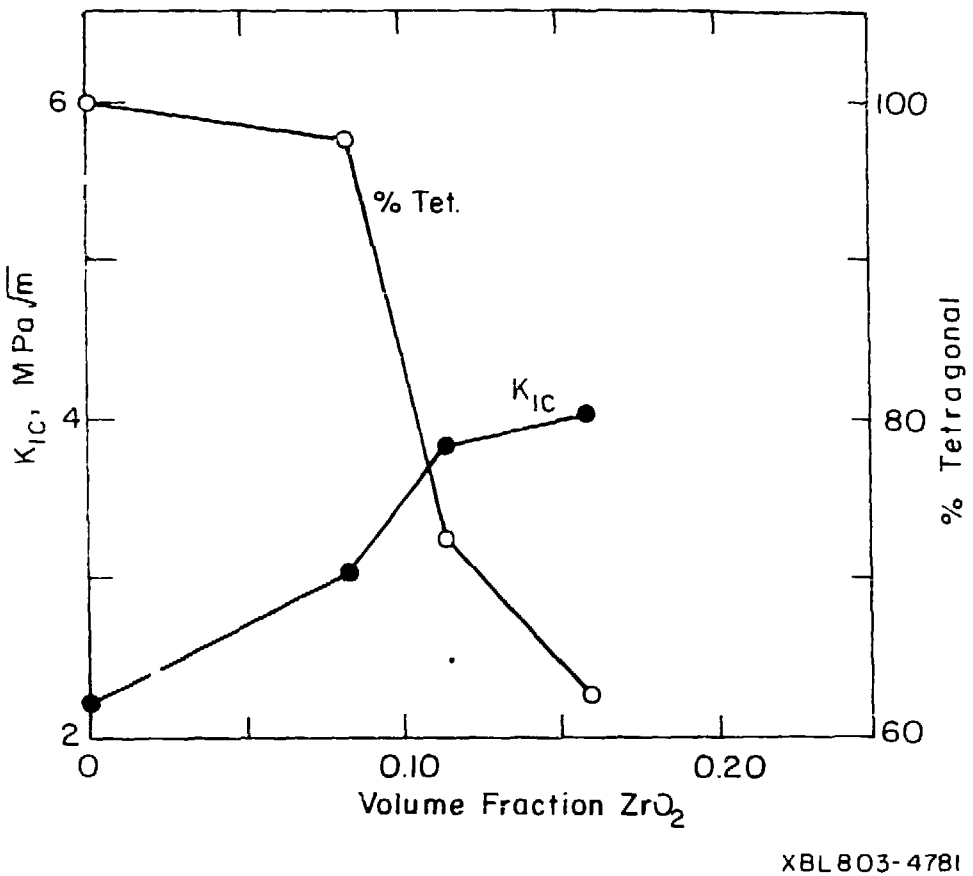
6
4
2
100
80
60
% Tet.
K_{IC}
K_{IC}, MPa$\sqrt{m}$
% Tetragonal
0
0.10
0.20
Volume Fraction ZrO_2
XBL803-4781

Fig. 10

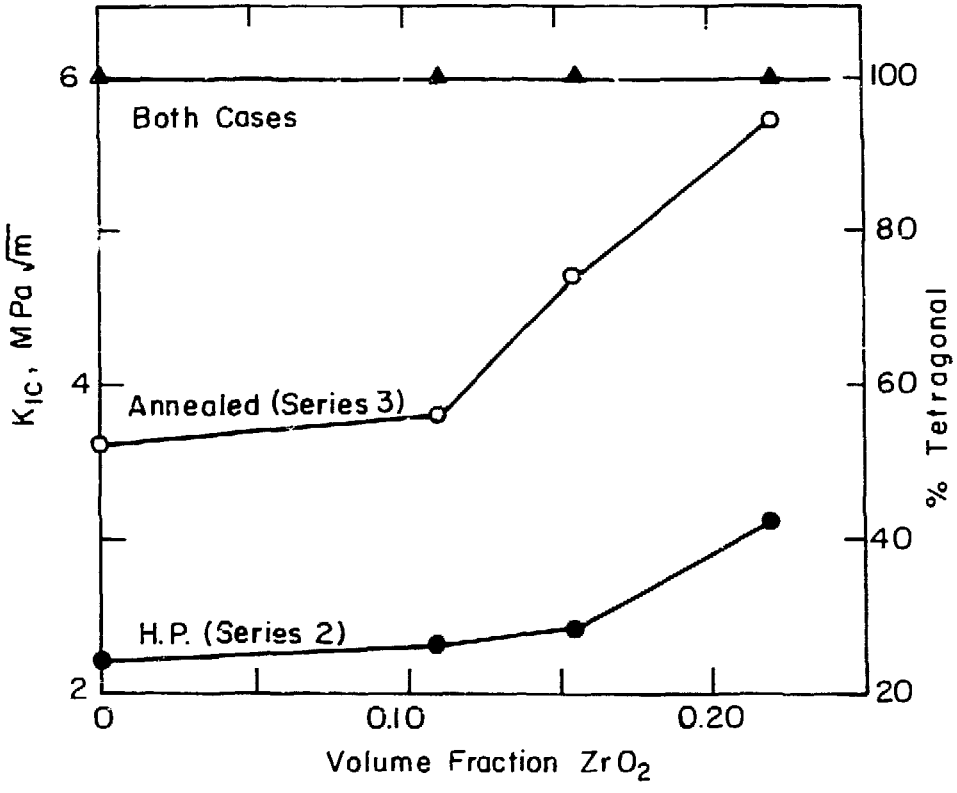
6
4
2
100
80
60
40
20
Both Cases
Annealed (Series 3)
H.P. (Series 2)
K_{IC}, MPa $\sqrt{m}$
% Tetragonal
0
0.10
0.20
Volume Fraction ZrO_2
XBL 803-4796

Fig. 11

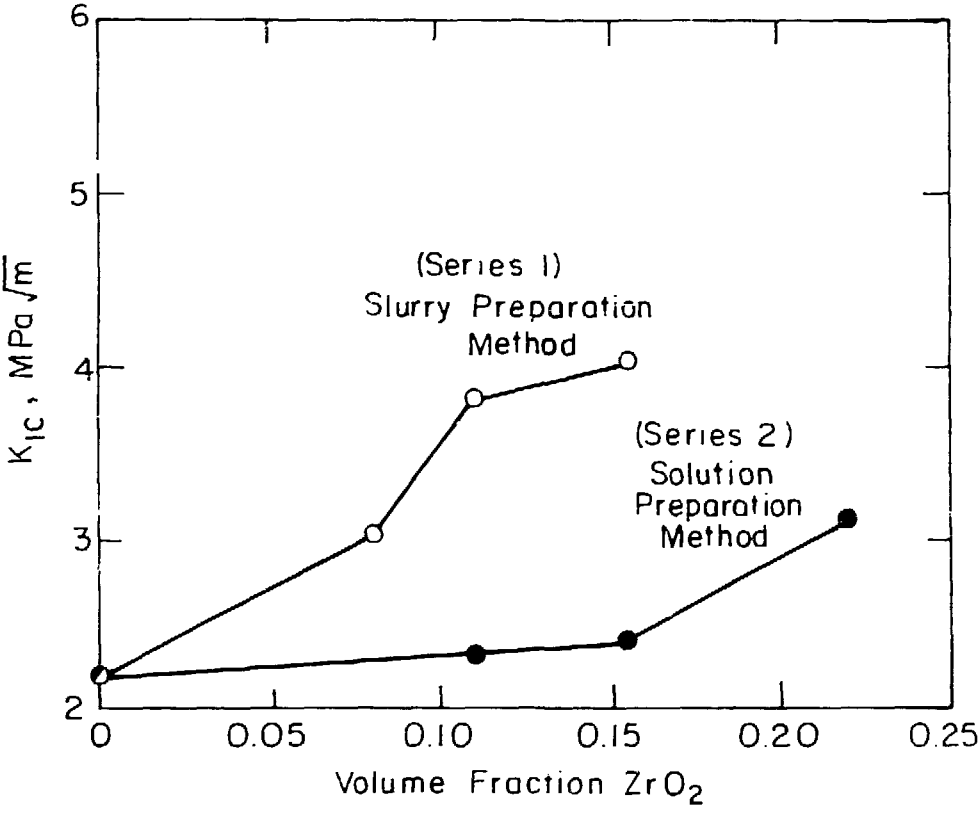
6
5
4
3
2
K_{IC}, MPa $\sqrt{m}$
(Series 1)
Slurry Preparation
Method
(Series 2)
Solution
Preparation
Method
0
0.05
0.10
0.15
0.20
0.25
Volume Fraction ZrO_2
XBL 803-4795

Fig. 1.

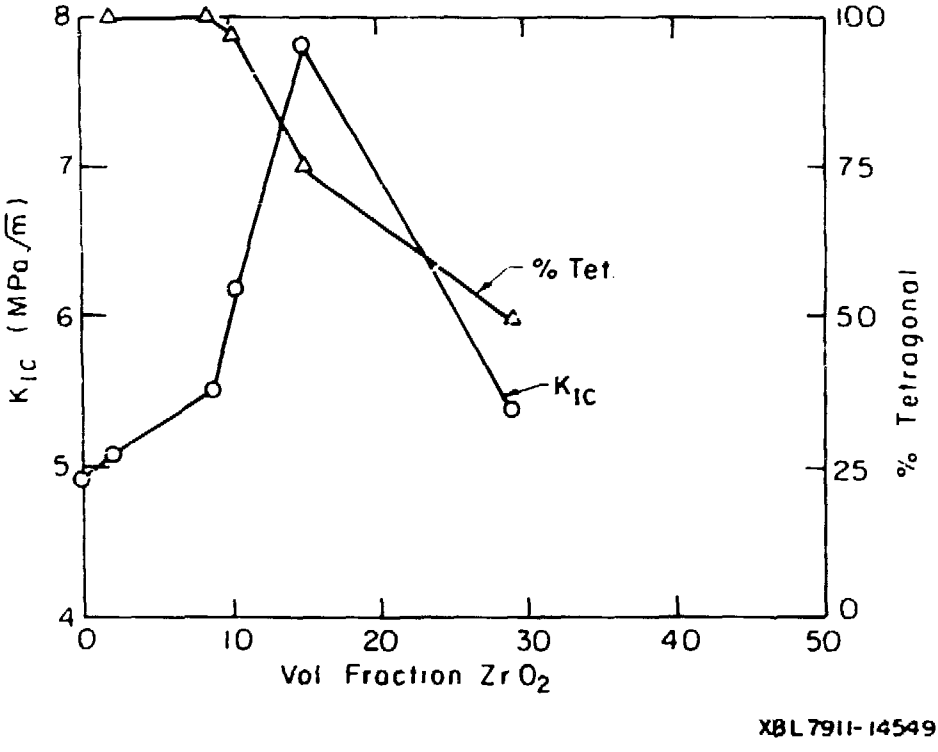
8
7
6
5
4
100
75
50
25
0
0
10
20
30
40
50
K_{IC} (MPa$\sqrt{m}$)
% Tetragonal
% Tet
K_{IC}
Vol Fraction ZrO_2
XBL7911-14549

Fig. 13

Fig. 14

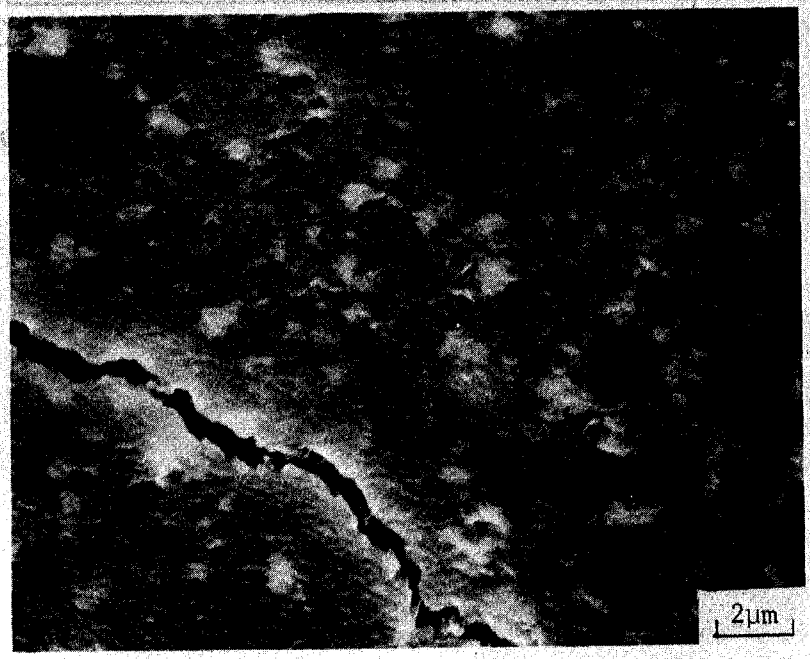

XBB 803-3499

Fig. 15

Matrix	$V_f(ZrO_2)$	b_o	k
Al_2O_3	.15	1.14	9
Al_2O_3	.08	.98	6
Mullite	.16	.35	10

Fig. 16

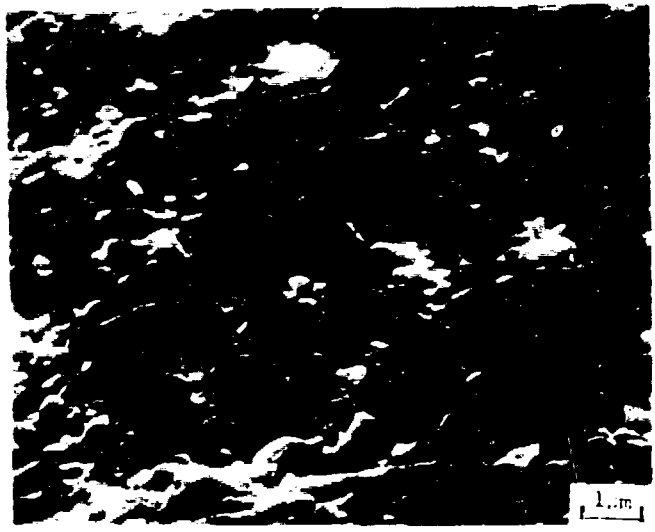

XBB 803-3500

Fig. 17

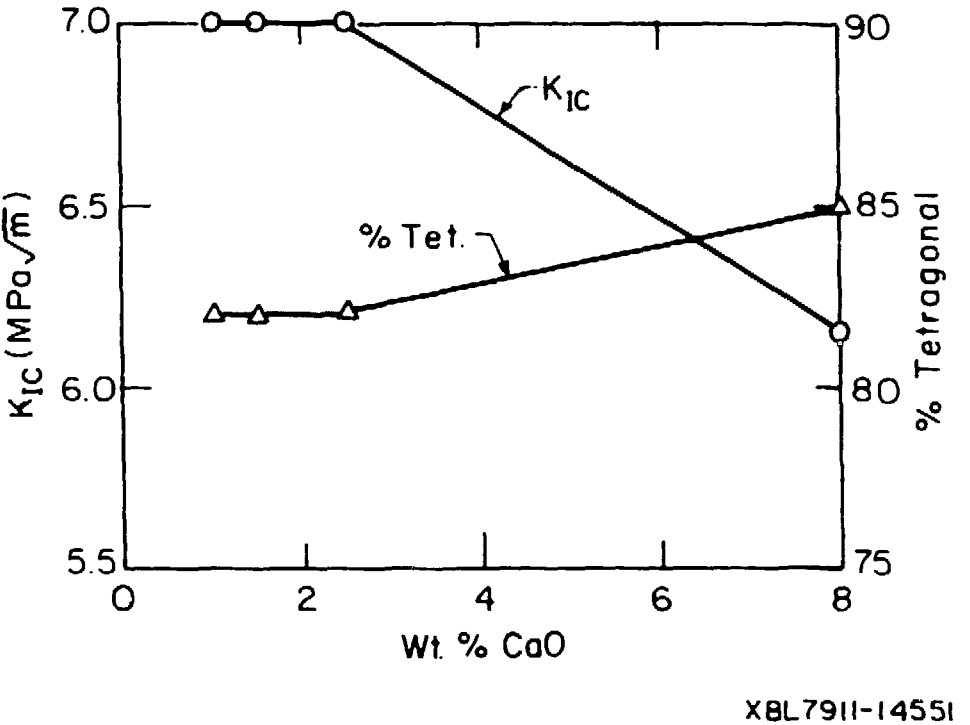
7.0
6.5
6.0
5.5
90
85
80
75
0
2
4
6
8
K_{IC}
% Tet.
K_{IC} (MPa$\sqrt{m}$)
% Tetragonal
Wt. % CaO
XBL7911-14551

Fig. 18

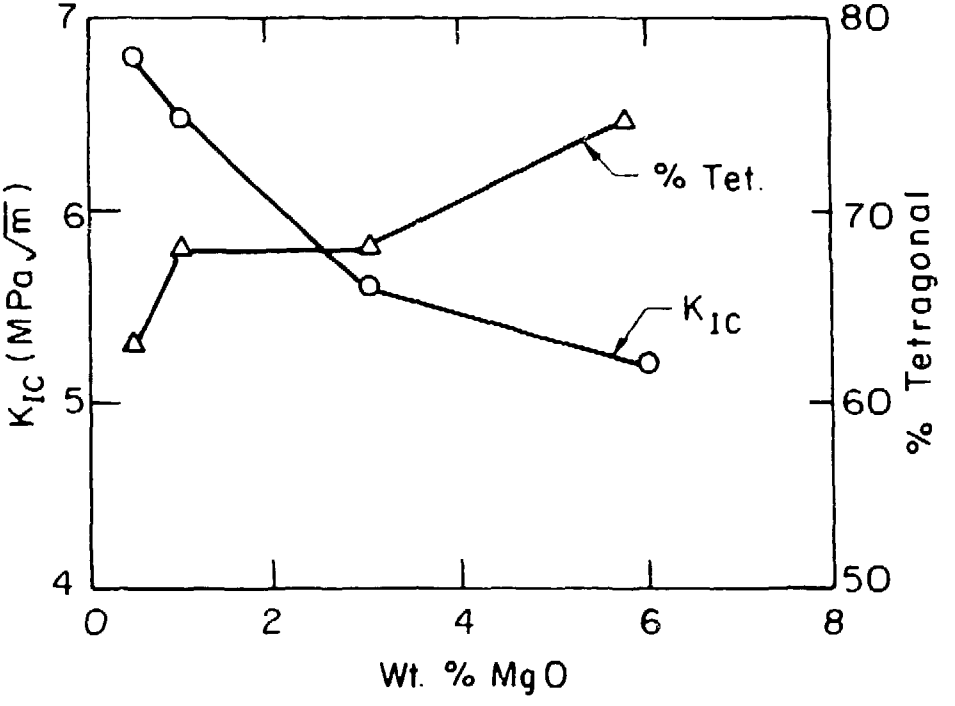

XBL 7911-14550

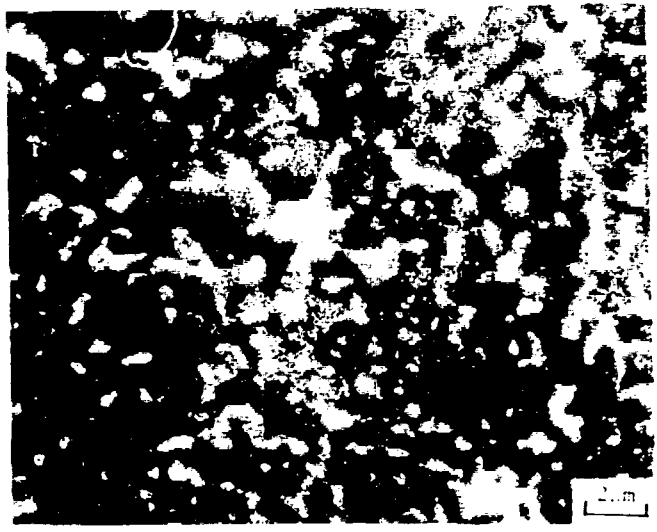

Fig. 20

XBB 803-3502

Fig. 21

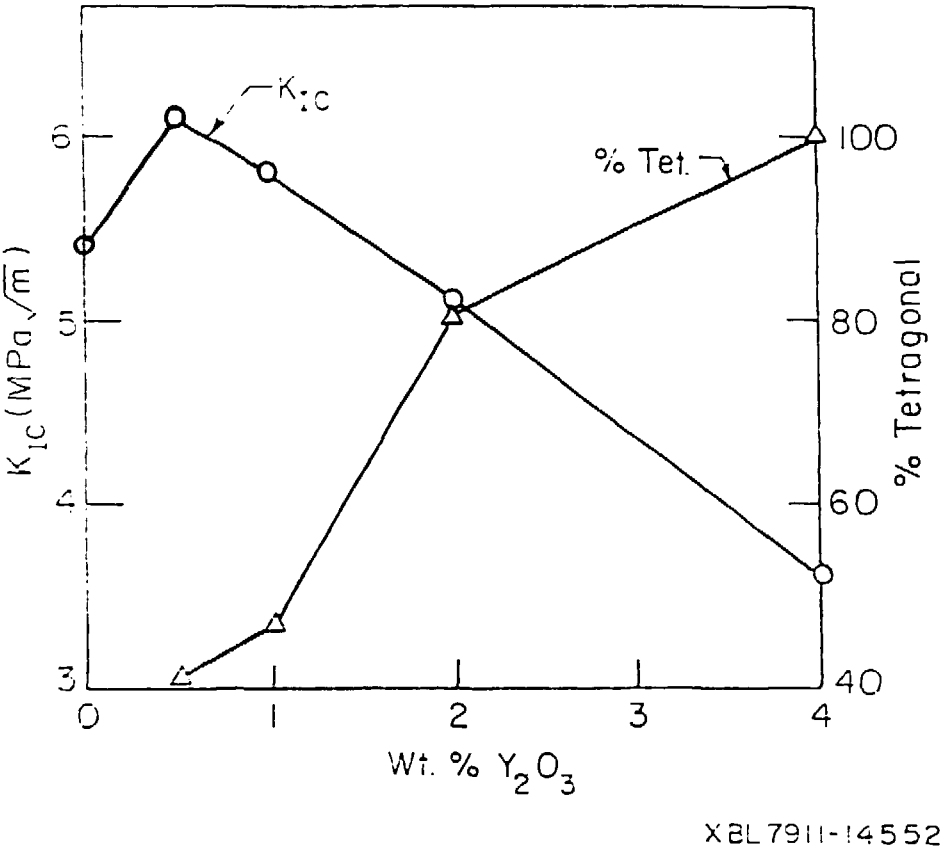
K_{IC}
% Tet.
100
80
60
40
% Tetragonal
K_{IC} (MPa$\sqrt{m}$)
6
5
4
3
0
1
2
3
4
Wt. % Y_2O_3
X8L7911-14552

Fig. 22

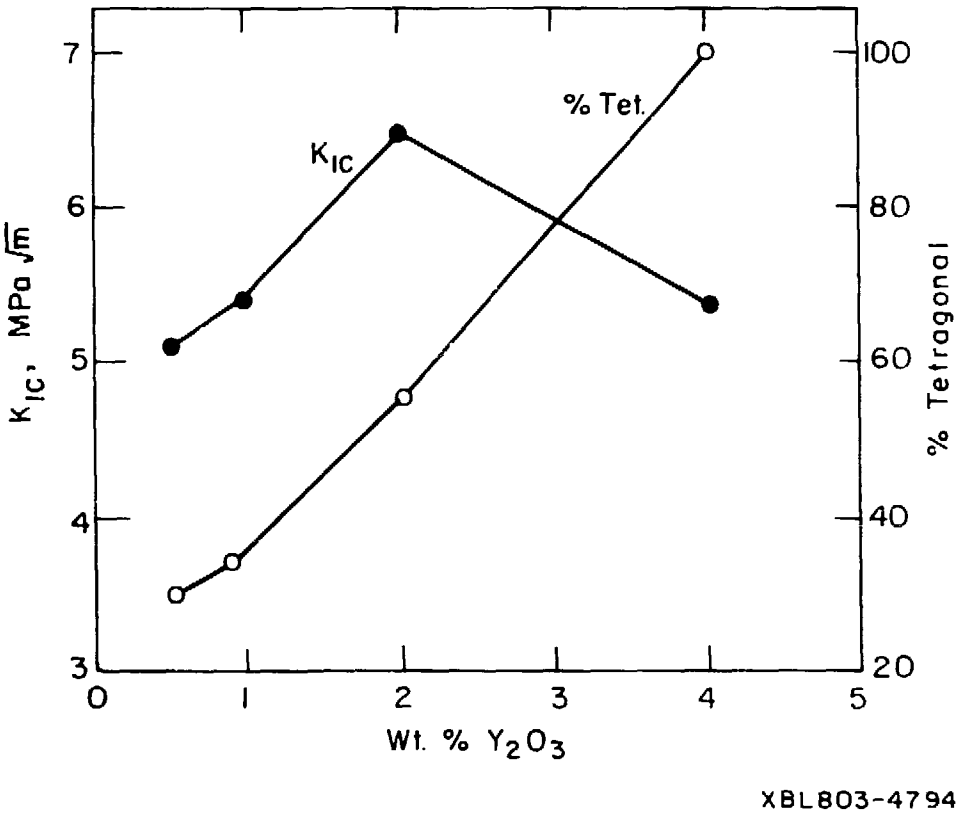
7
6
5
4
3
0
1
2
3
4
5
100
80
60
40
20
% Tet.
K_{IC}
K_{IC}, MPa $\sqrt{m}$
% Tetragonal
Wt. % Y_2O_3
XBL803-4794

Fig. 23

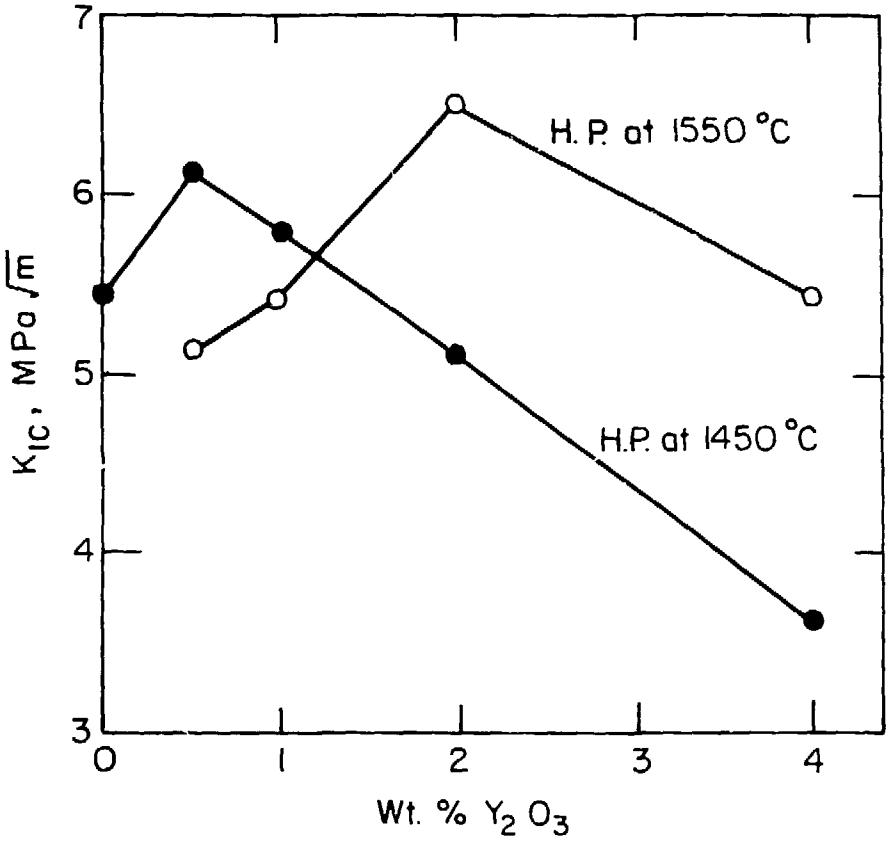

XBL 803-4797

Fig. 24

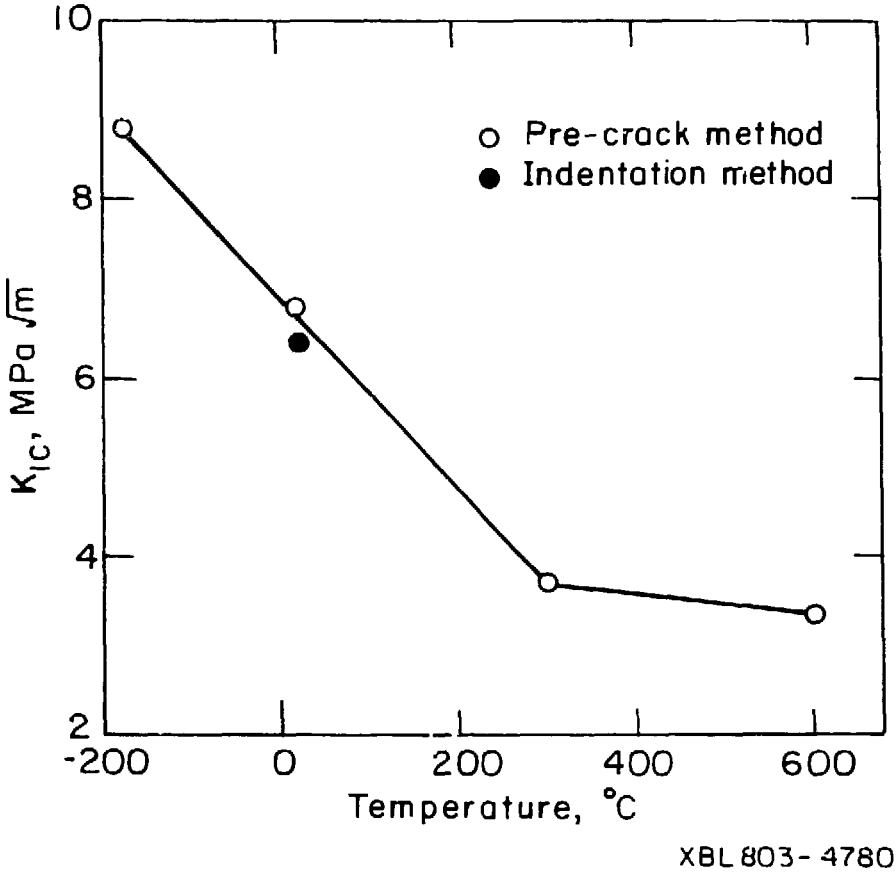
10
8
6
4
2
K_{IC}, MPa $\sqrt{m}$
Pre-crack method
Indentation method
-200
0
200
400
600
Temperature, °C
XBL 803-4780

Fig. 25

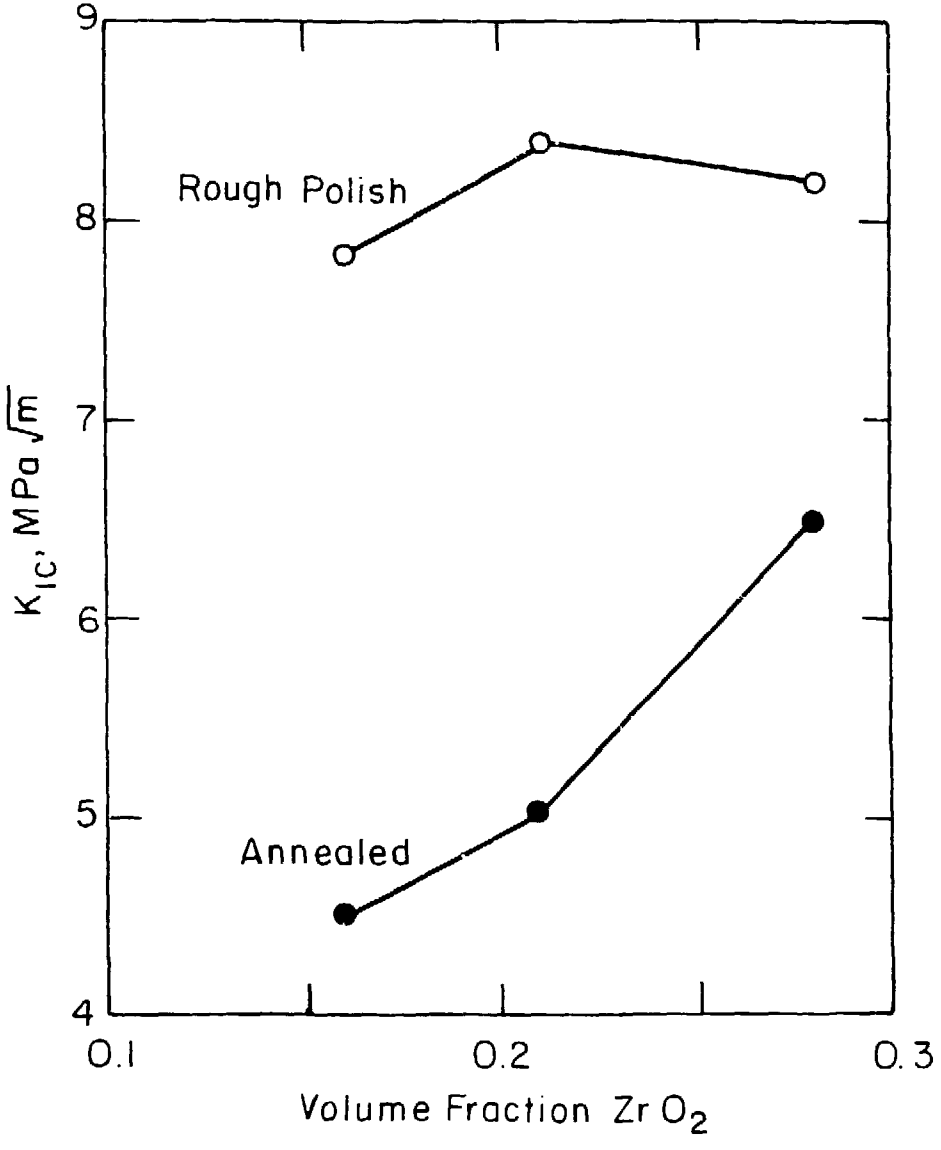
9
8
7
6
5
4
Rough Polish
Annealed
K_{IC}, MPa $\sqrt{m}$
0.1
0.2
0.3
Volume Fraction ZrO_2
XBL 803-4789

Fig. 26

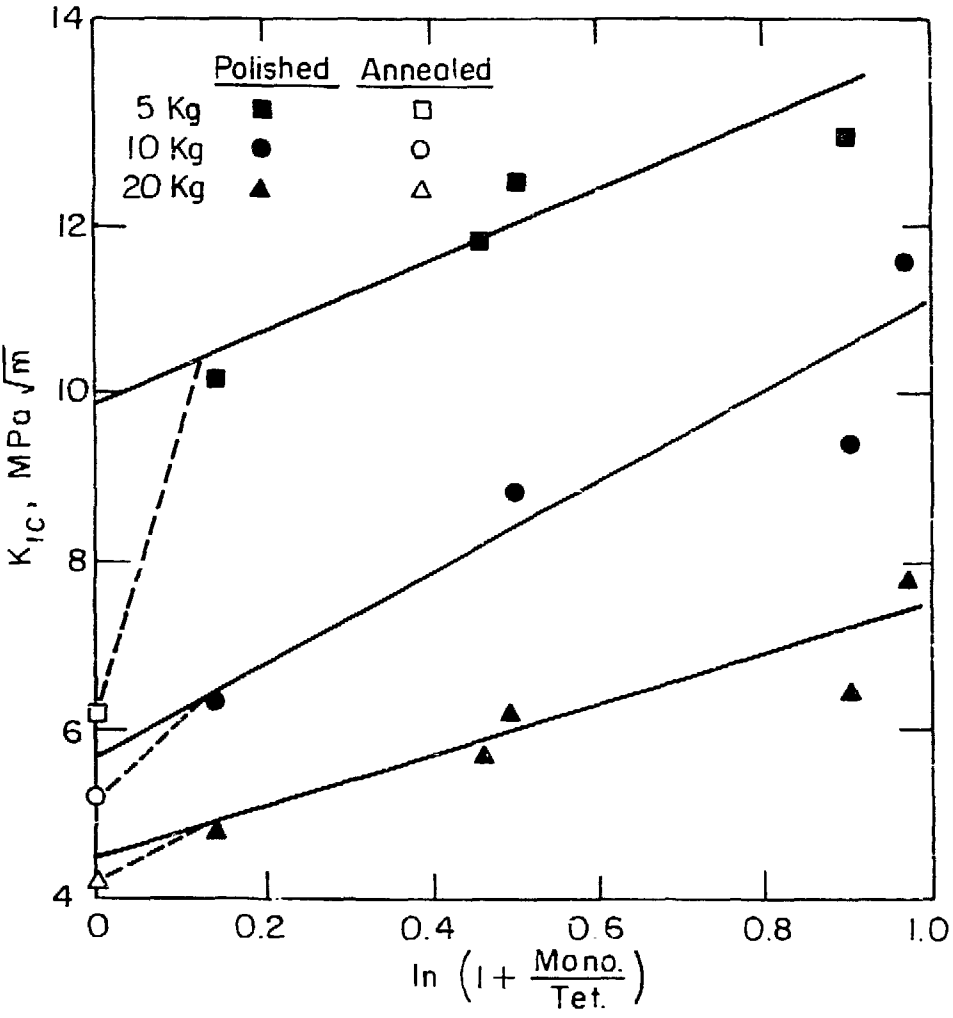
Polished
Annealed
5 Kg
10 Kg
20 Kg
14
12
10
8
6
4
K_{IC}, MPa $\sqrt{m}$
0
0.2
0.4
0.6
0.8
1.0
$\ln\left(1+\frac{\text{Mono.}}{\text{Tet.}}\right)$

XBL803-4793

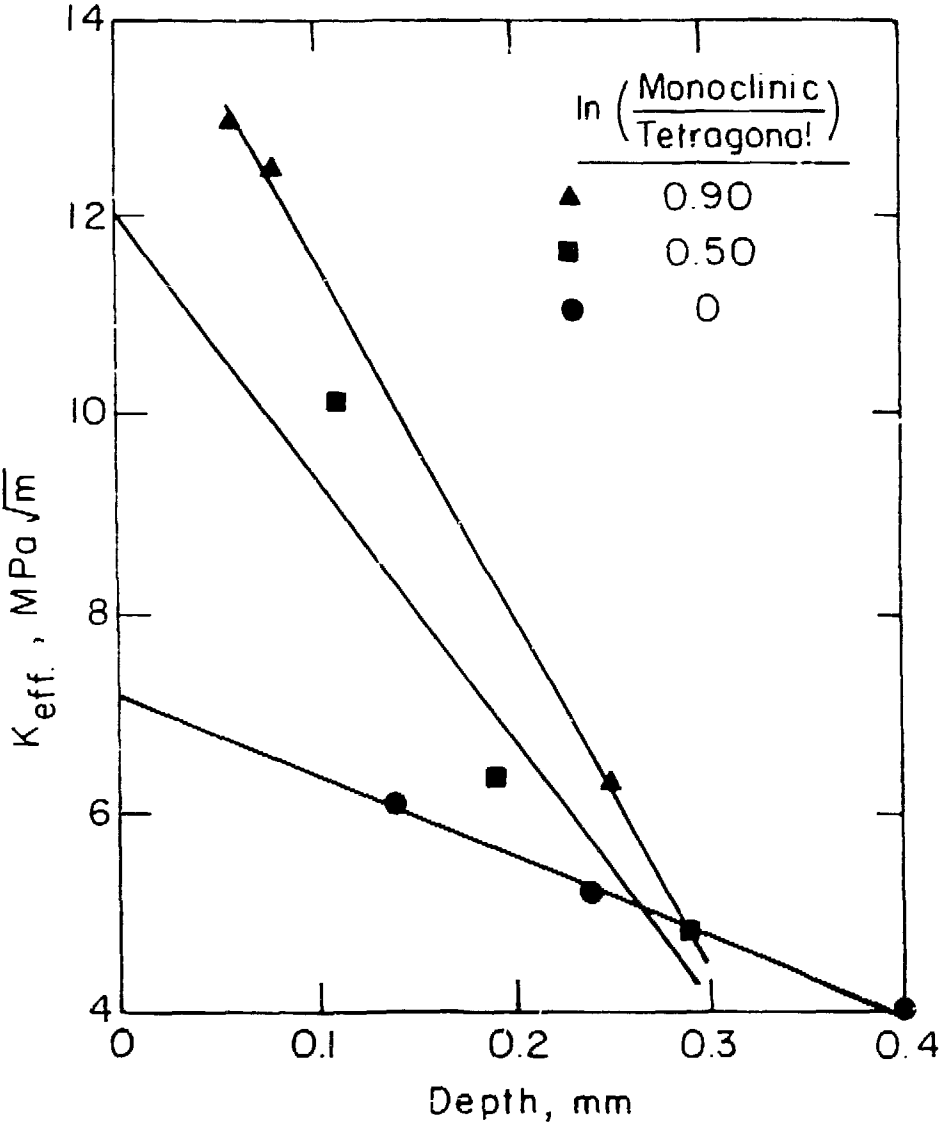
14
12
10
8
6
4
0
0.1
0.2
0.3
0.4
$K_{eff.}$, MPa$\sqrt{m}$
Depth, mm
$\ln\left(\frac{\text{Monoclinic}}{\text{Tetragonal}}\right)$
0.90
0.50
0

XBL803-4787

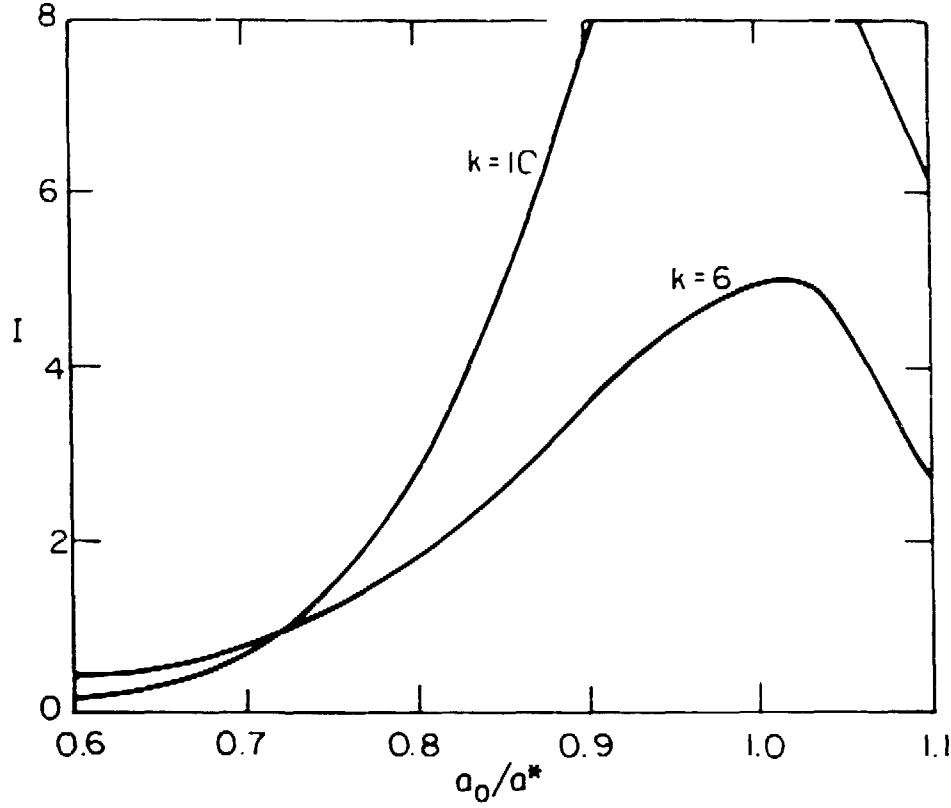
8
6
4
2
0
I
k = 10
k = 6
0.6
0.7
0.8
0.9
1.0
1.1
a_0/a^*
XBL803-4786

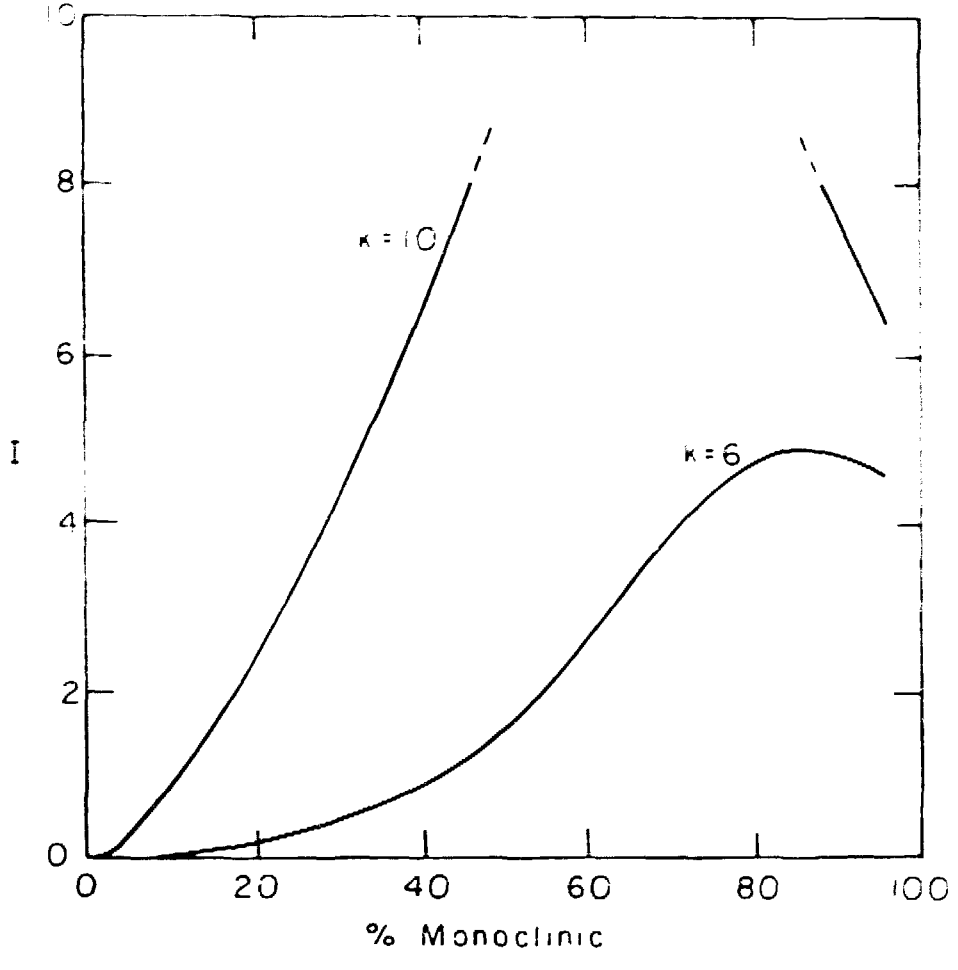

XBL803-4790

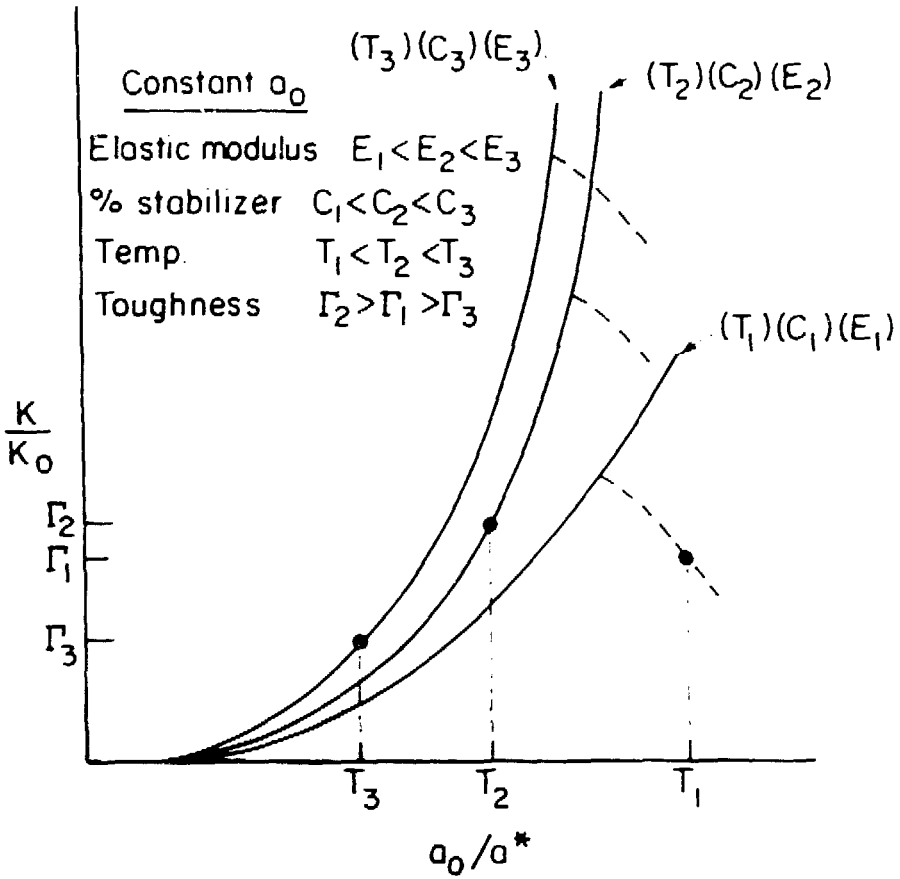
Constant a_0
Elastic modulus $E_1 < E_2 < E_3$
% stabilizer $C_1 < C_2 < C_3$
Temp. $T_1 < T_2 < T_3$
Toughness $\Gamma_2 > \Gamma_1 > \Gamma_3$
$(T_3)(C_3)(E_3)$
$(T_2)(C_2)(E_2)$
$(T_1)(C_1)(E_1)$
$\frac{K}{K_0}$
Γ_2
Γ_1
Γ_3
T_3
T_2
T_1
a_0/a^*

XBL 803-4821

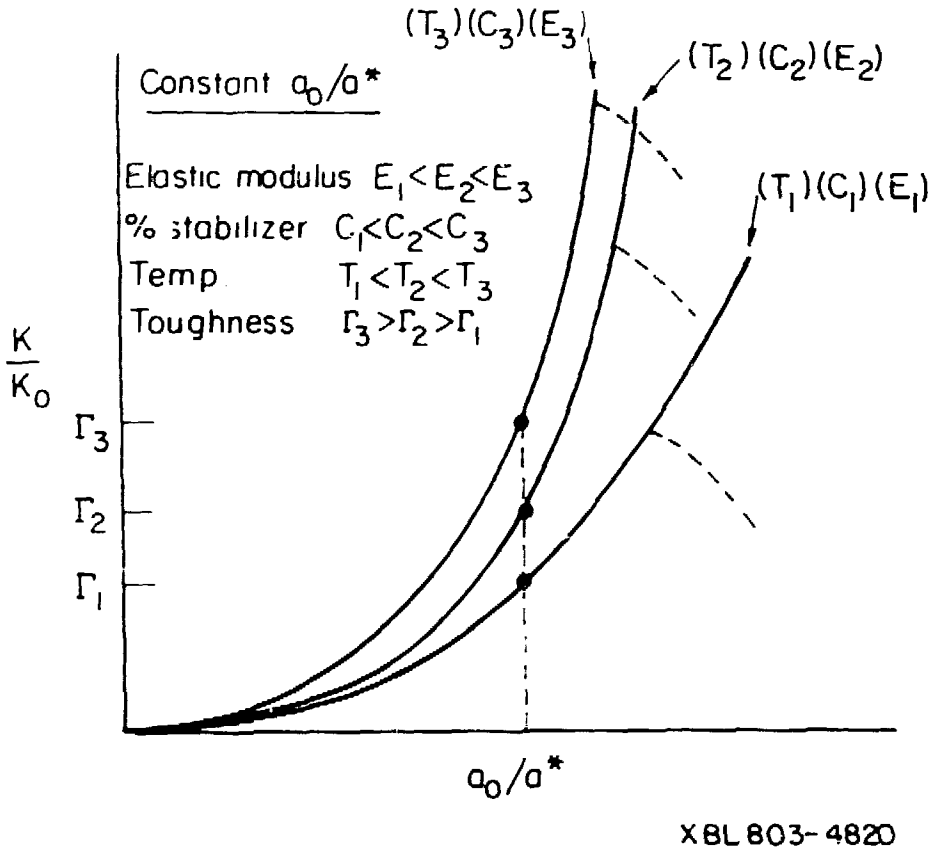
$(T_3)(C_3)(E_3)$
$(T_2)(C_2)(E_2)$
$(T_1)(C_1)(E_1)$
Constant a_0/a^*
Elastic modulus $E_1<E_2<E_3$
% stabilizer $C_1<C_2<C_3$
Temp $T_1<T_2<T_3$
Toughness $\Gamma_3>\Gamma_2>\Gamma_1$
$\frac{K}{K_0}$
Γ_3
Γ_2
Γ_1
a_0/a^*

XBL 803-4820

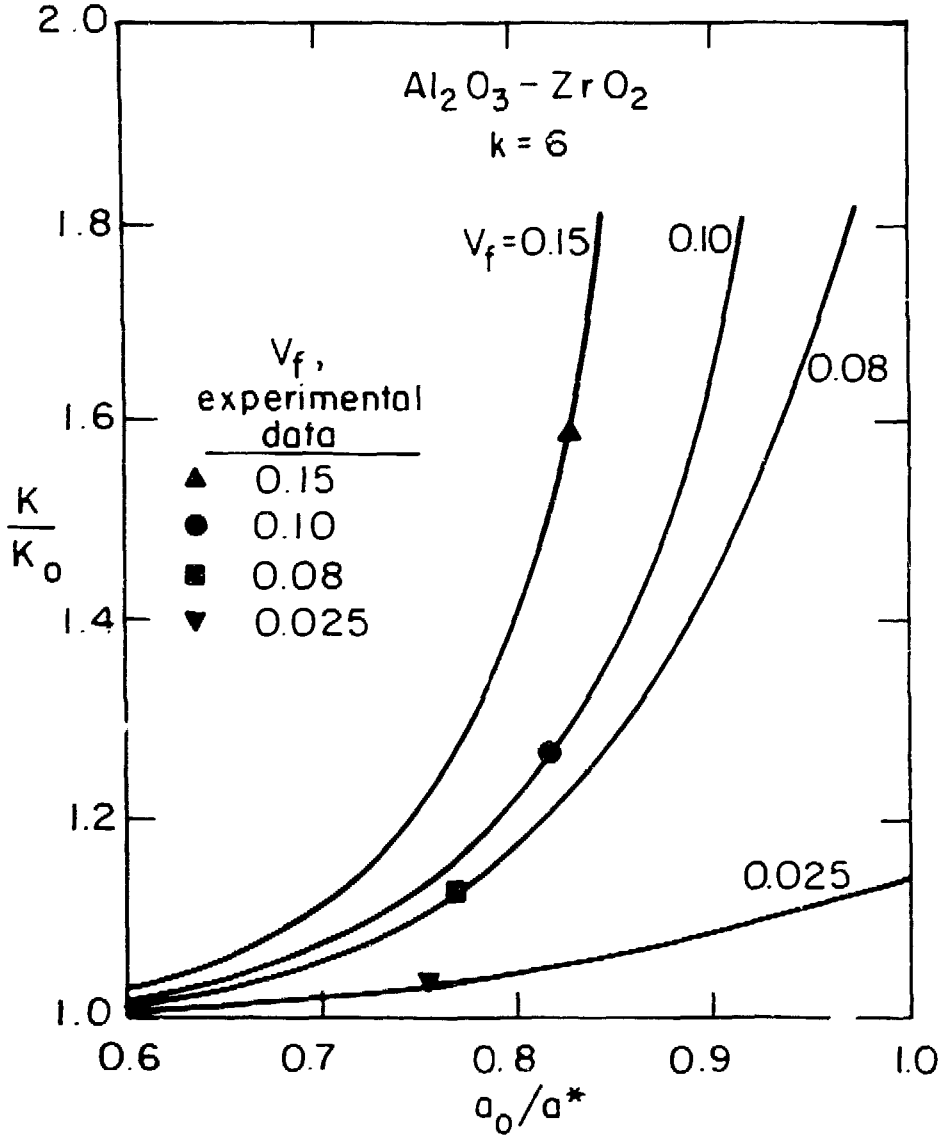
2.0
1.8
1.6
1.4
1.2
1.0
K/K0
Al2O3 - ZrO2
k = 6
Vf = 0.15
0.10
0.08
0.025
Vf, experimental data
0.15
0.10
0.08
0.025
0.6
0.7
0.8
0.9
1.0
a0/a*
XBL803-4792

Fig. 33

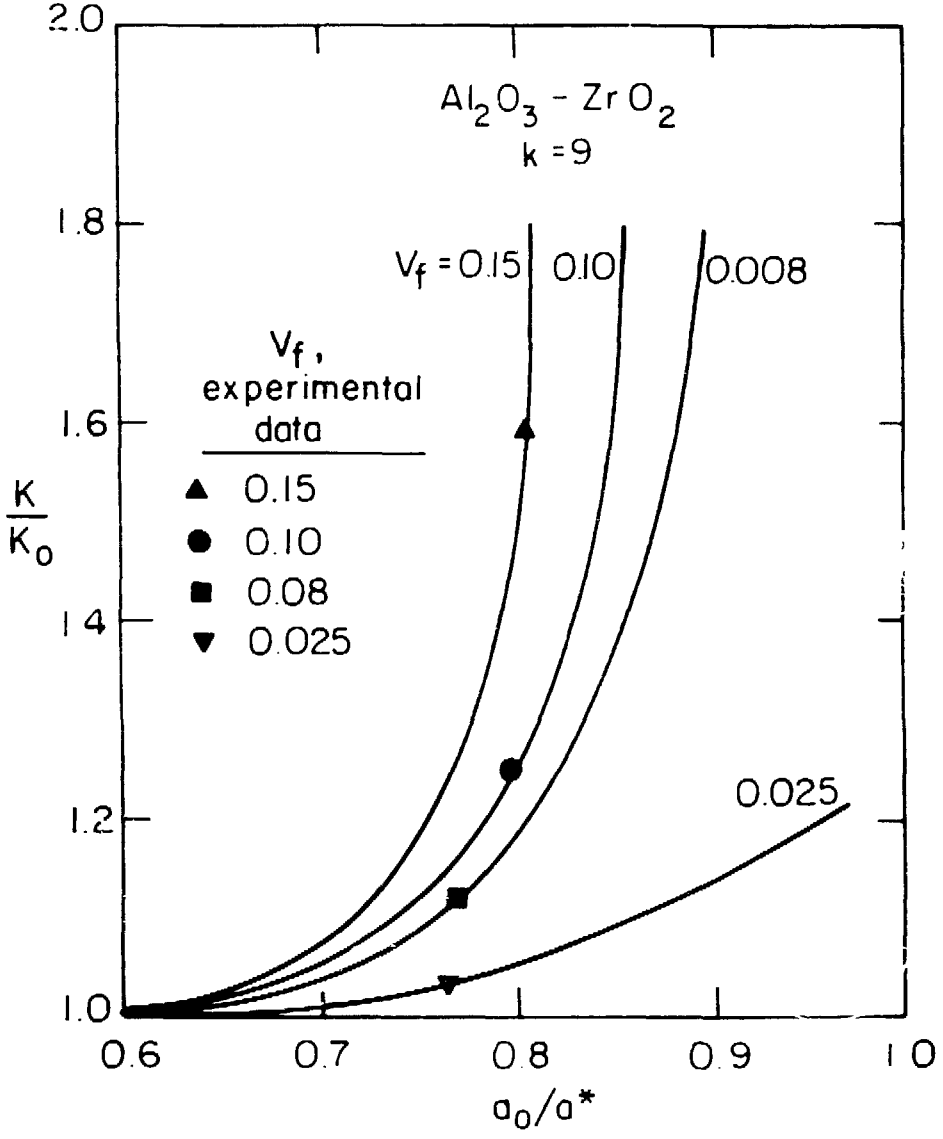
2.0
1.8
1.6
1.4
1.2
1.0
K/K0
Al2O3 - ZrO2
k = 9
Vf = 0.15
0.10
0.008
0.025
Vf, experimental data
0.15
0.10
0.08
0.025
0.6
0.7
0.8
0.9
1.0
a0/a*

XBL 803-4791

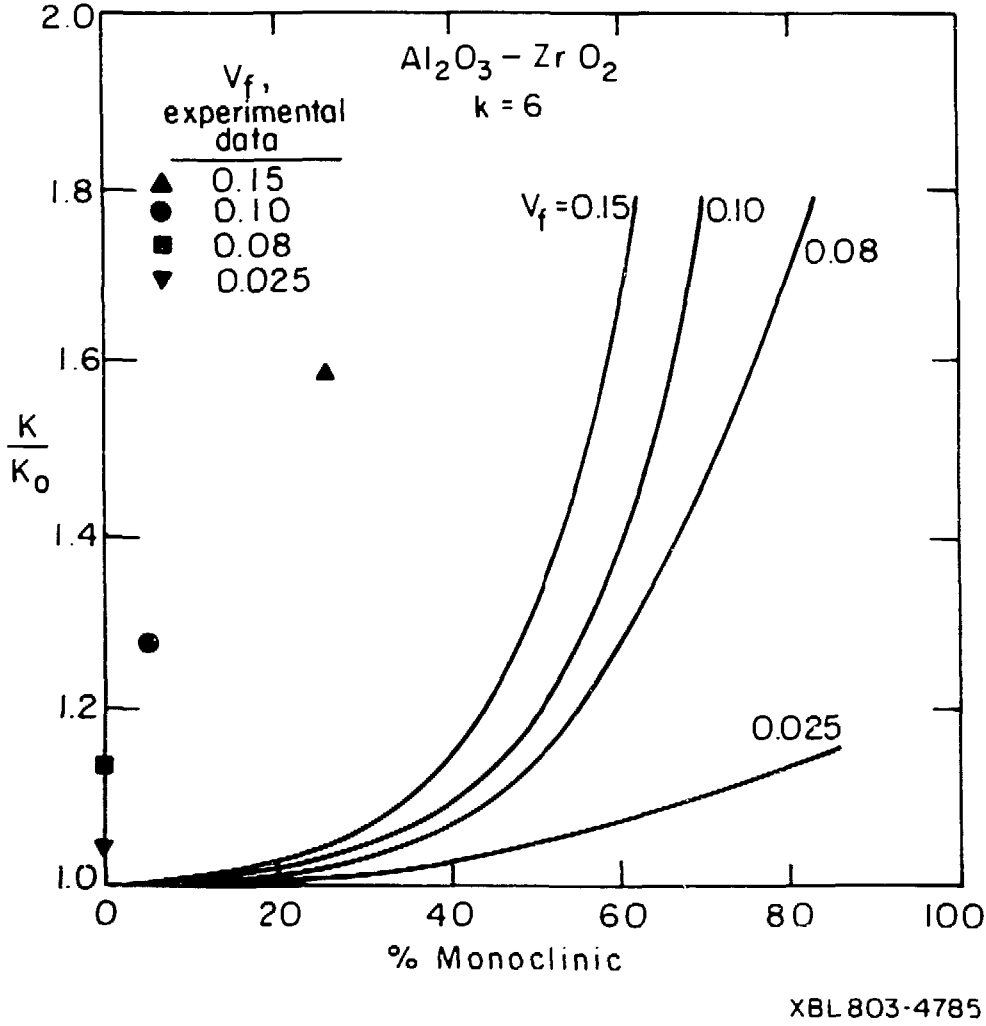
2.0
1.8
1.6
1.4
1.2
1.0
K/K0
Al2O3 – Zr O2
k = 6
Vf, experimental data
0.15
0.10
0.08
0.025
Vf =0.15
0.10
0.08
0.025
0
20
40
60
80
100
% Monoclinic
XBL 803-4785

Fig. 35

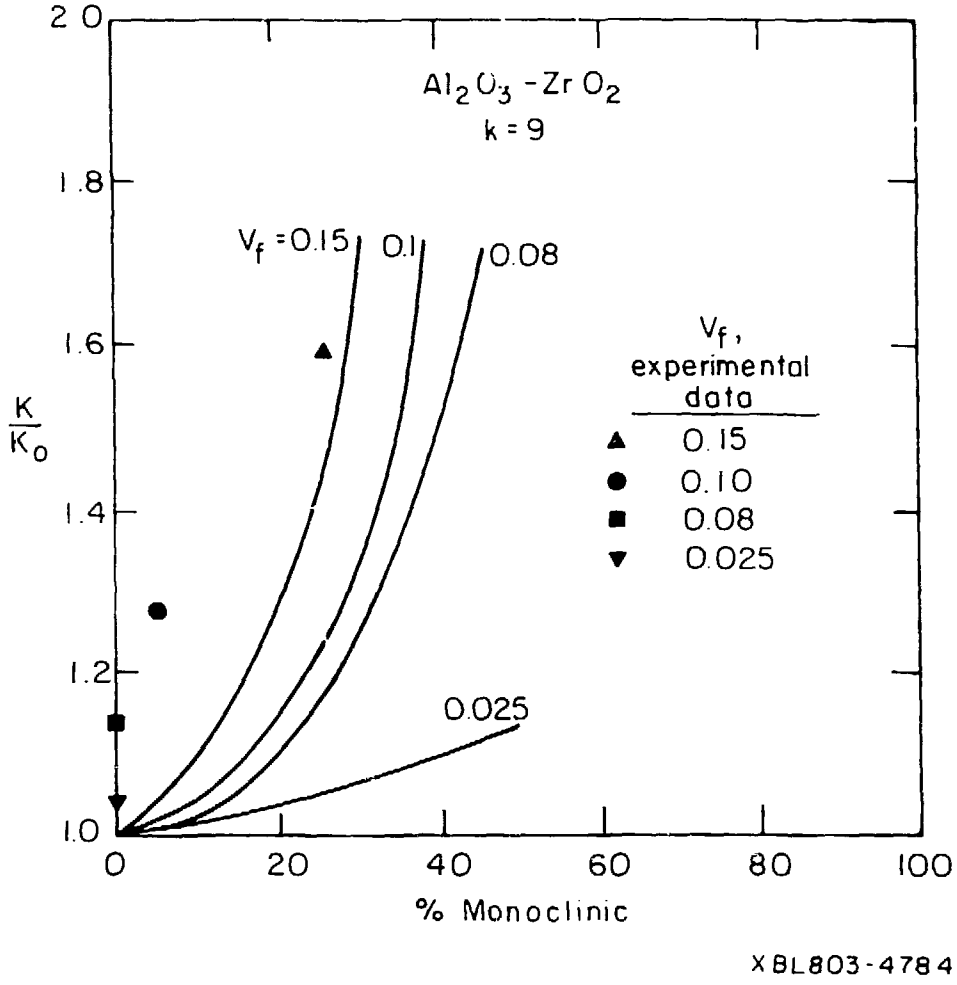
2.0
1.8
1.6
1.4
1.2
1.0
K/K0
Al2O3 - ZrO2
k = 9
Vf = 0.15
0.1
0.08
0.025
Vf, experimental data
0.15
0.10
0.08
0.025
0
20
40
60
80
100
% Monoclinic
XBL803-4784

Fig. 36

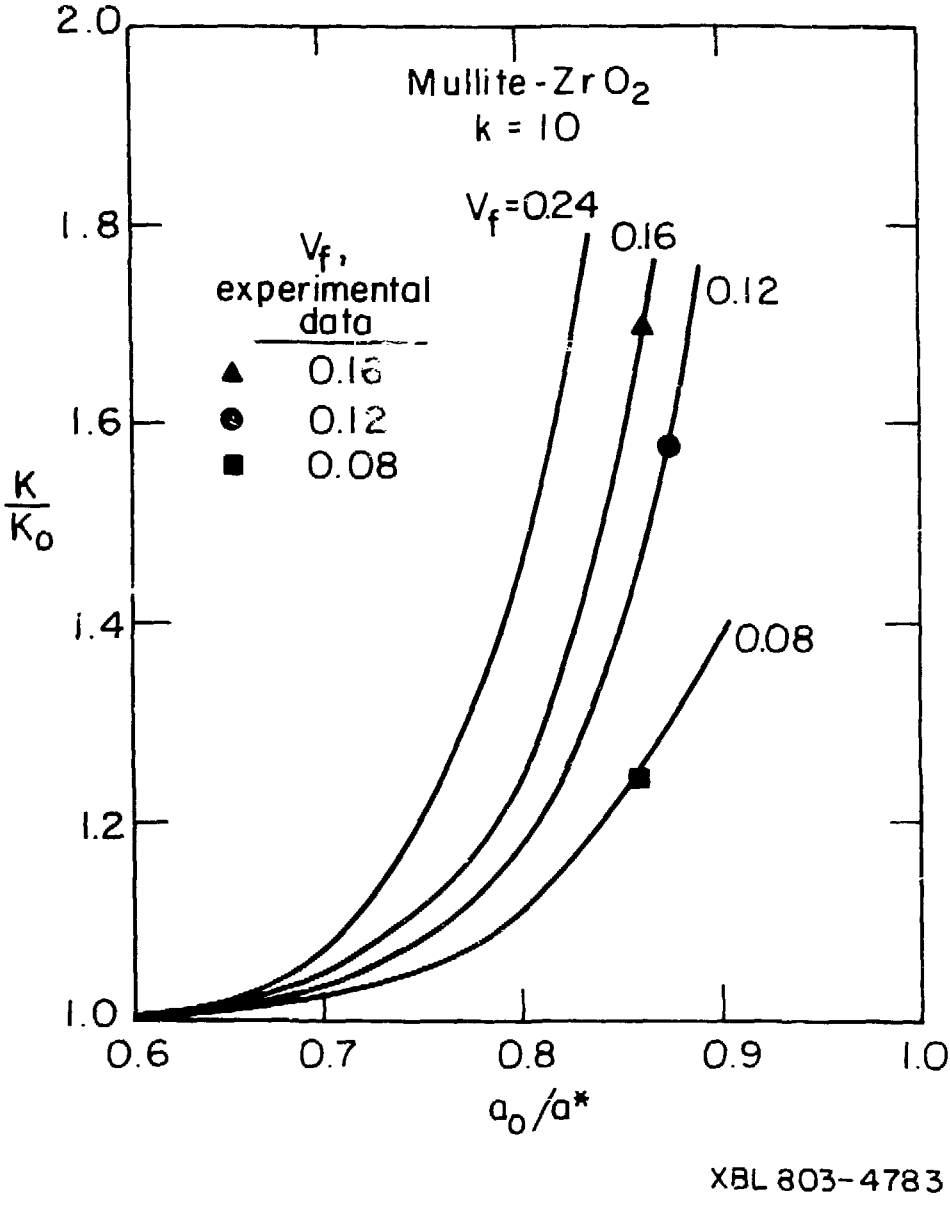
Mullite - ZrO_2
k = 10
V_f=0.24
0.16
0.12
0.08
V_f, experimental data
0.16
0.12
0.08
$\frac{K}{K_0}$
a_0/a^*
2.0
1.8
1.6
1.4
1.2
1.0
0.6
0.7
0.8
0.9
1.0
XBL 803-4783

Fig. 37

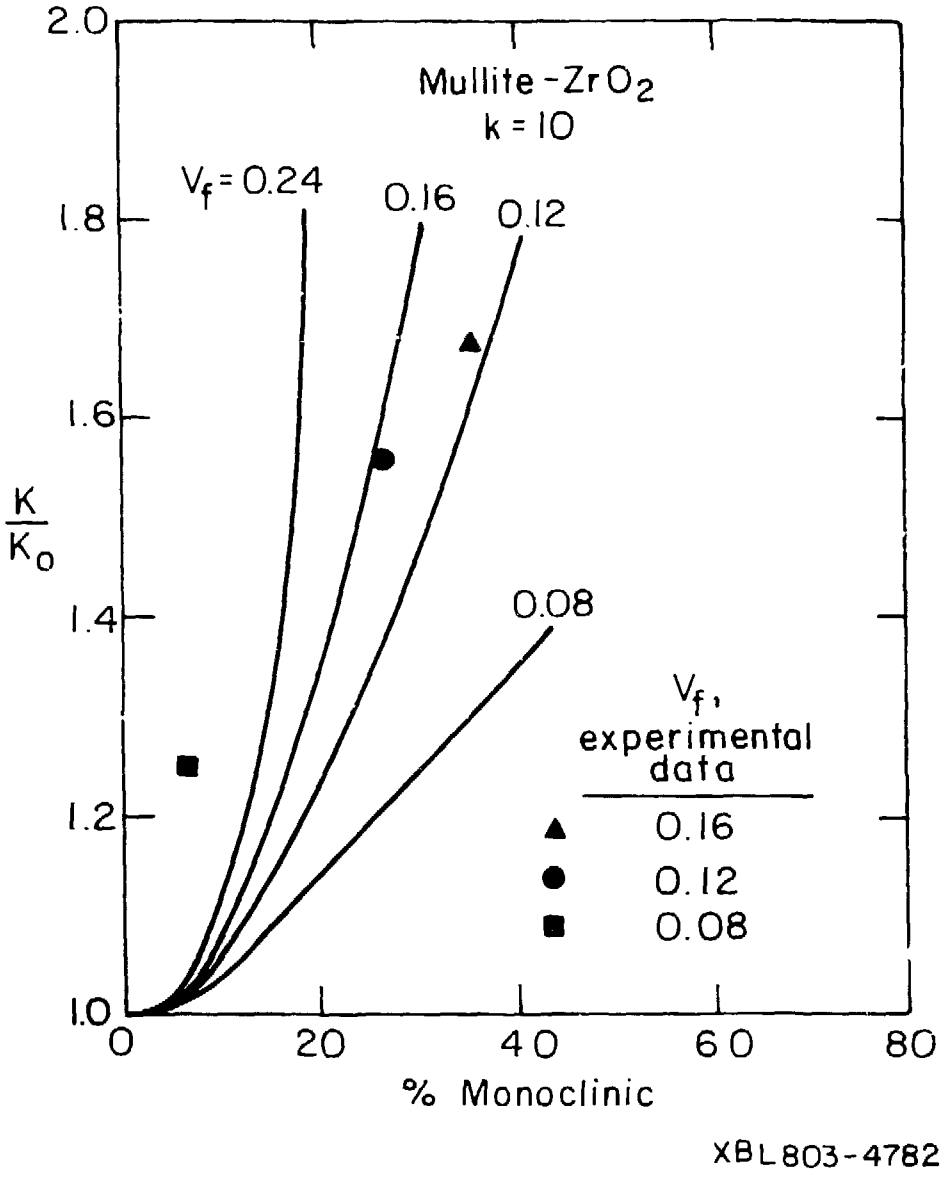
Mullite - ZrO_2
k = 10
V_f = 0.24
0.16
0.12
0.08
V_f, experimental data
0.16
0.12
0.08
$\frac{K}{K_o}$
2.0
1.8
1.6
1.4
1.2
1.0
0
20
40
60
80
% Monoclinic
XBL803-4782

Fig. 38

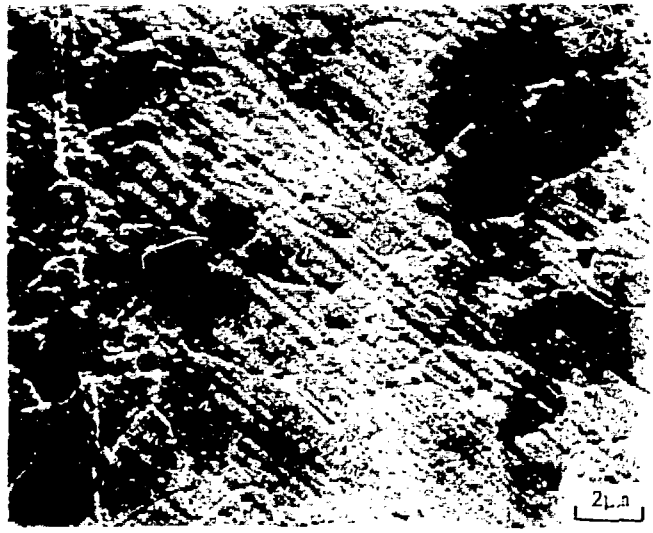

XBB 803-3503

Fig. 39

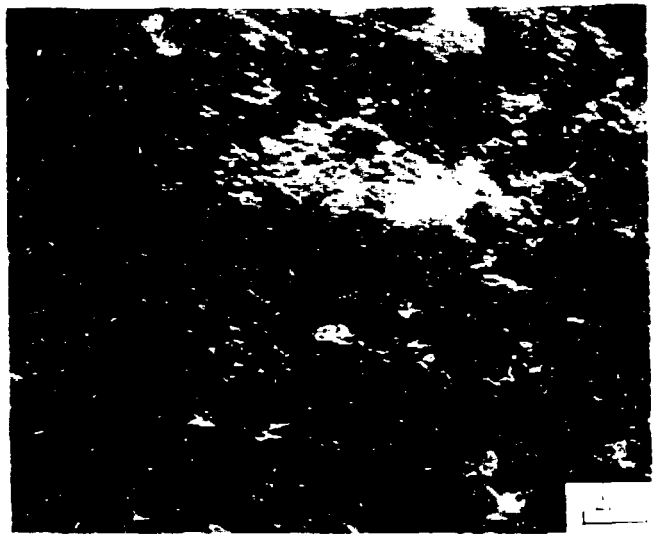

Fig. 40

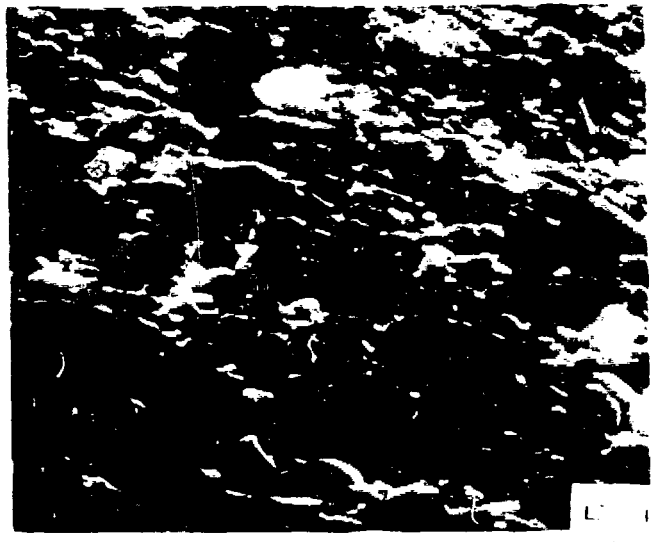

XBB 803-3504

Fig. 41

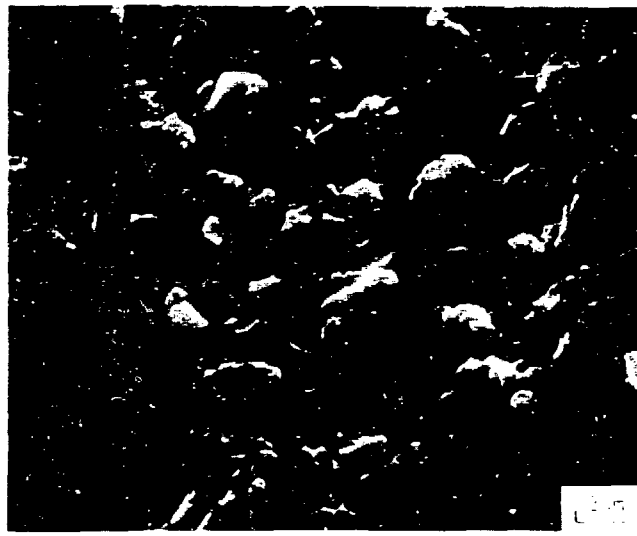

Fig. 42

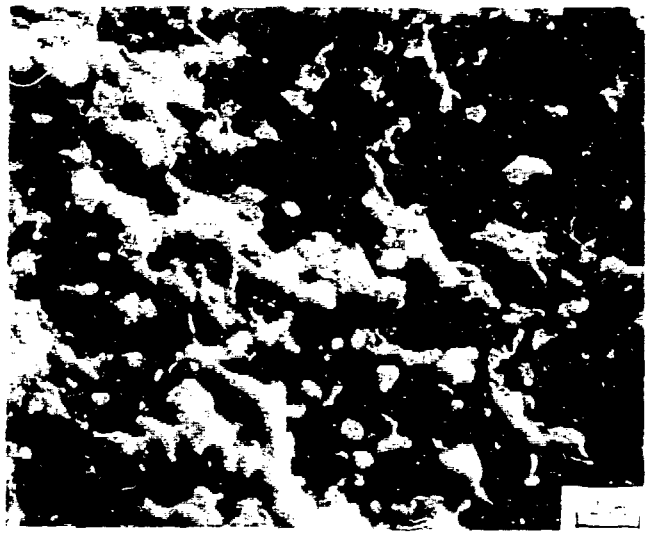

XBB 803-3501

Fig. 43

Fig. A1

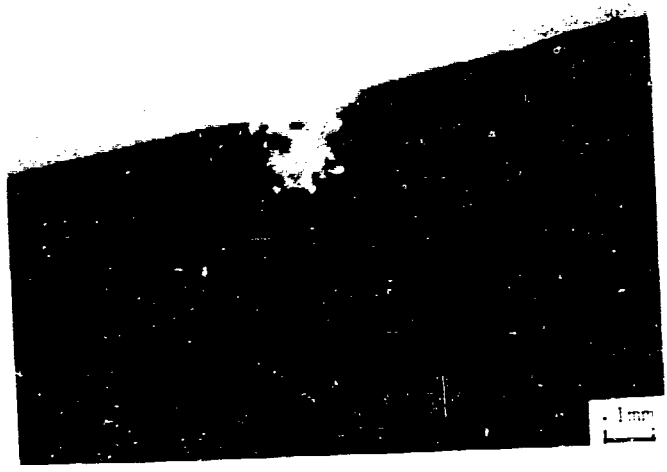

XBB 803-3505

Fig. A2

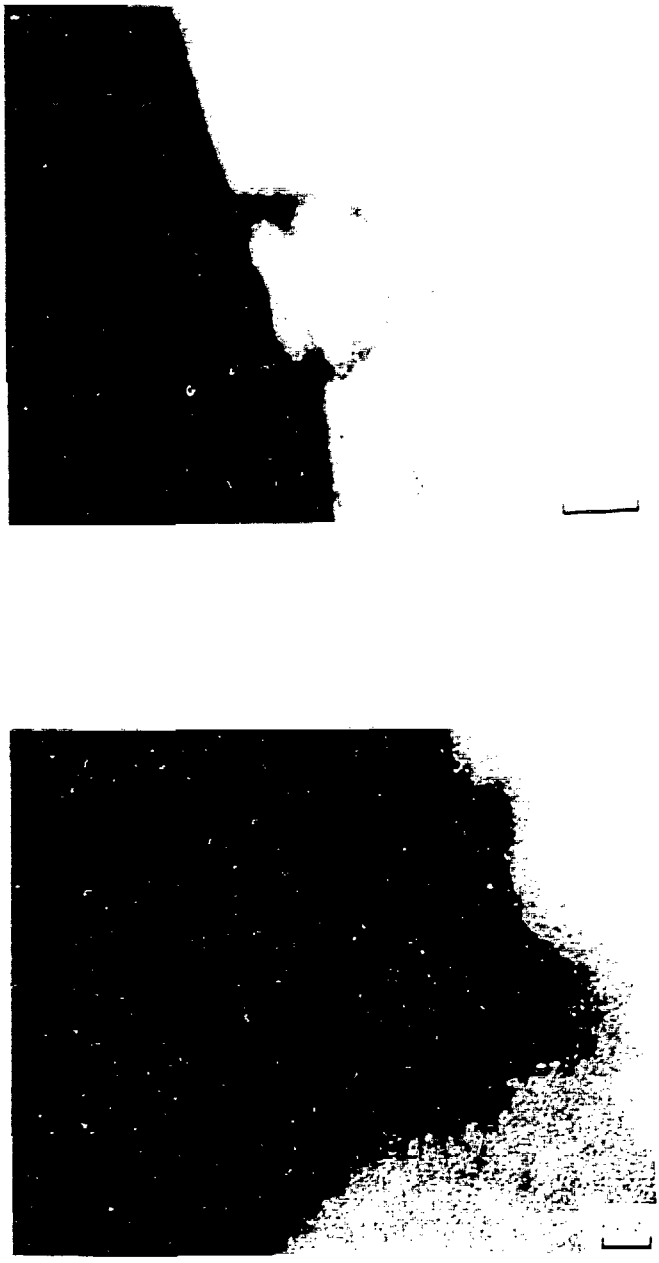

XBB 803-3506

Fig. 3